

BOLU ABANT IZZET BAYSAL UNIVERSITY
THE GRADUATE SCHOOL OF NATURAL AND APPLIED
SCIENCES
DEPARTMENT OF CHEMISTRY



EFFECT OF SURFACTANT ALKYL CHAIN LENGTH ON
UNIAXIAL TO BIAXIAL CHOLESTERIC PHASE
TRANSITIONS IN LYOTROPIC MIXTURES

MASTER OF SCIENCE

SEDA UYANIK

BOLU, JUNE 2019

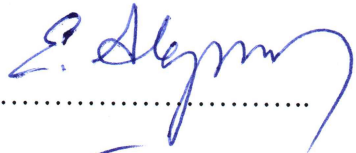
APPROVAL OF THE THESIS

EFFECT OF SURFACTANT ALKYL CHAIN LENGTH ON UNIAXIAL TO BIAXIAL CHOLESTERIC PHASE TRANSITIONS IN LYOTROPIC MIXTURES submitted by **SEDA UYANIK** in partial fulfillment of the requirements for the degree of **Master of Science** in **Department of Chemistry, The Graduate School of Natural and Applied Sciences of BOLU ABANT IZZET BAYSAL UNIVERSITY** in 26/06/2019 by

Examining Committee Members

Signature

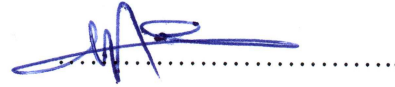
Supervisor
Assoc. Prof. Dr. Erol AKPINAR
Bolu Abant Izzet Baysal University



Member
Assoc. Prof. Dr. Öznur DEMİR ORDU
Bolu Abant Izzet Baysal University



Member
Assoc. Prof. Dr. Mecit AKSU
Duzce University



Graduation Date :

Prof. Dr. Ömer ÖZYURT

Director of Graduate School of Natural and Applied Sciences





To my family

DECLARATION

I hereby declare that all information in this document has been obtained and presented in accordance with academic rules and ethical conduct. I also declare that, as required by these rules and conduct, I have fully cited and referenced all material and results that are not original to this work.

SEDA UYANIK

S. Uyanik

ABSTRACT

EFFECT OF SURFACTANT ALKYL CHAIN LENGTH ON UNIAXIAL TO BIAXIAL CHOLESTERIC PHASE TRANSITIONS IN LYOTROPIC

MIXTURES

MSC THESIS

SEDA UYANIK

**BOLU ABANT IZZET BAYSAL UNIVERSITY GRADUATE SCHOOL OF
NATURAL AND APPLIED SCIENCES**

DEPARTMENT OF CHEMISTRY

(SUPERVISOR: ASSOC. PROF. DR. EROL AKPINAR)

BOLU, JUNE 2019

In the present work, some ionic surfactant-based lyotropic mixtures, exhibiting cholesteric phases, were prepared to investigate the effect of surfactant alkyl chain length on (a) uniaxial-to-biaxial phase transitions and (b) stabilization of different cholesteric phases. Potassium alkanoates, KC_x , (potassium undecanoate, KC_{11} , potassium dodecanoate, KC_{12} , and potassium tridecanoate, KC_{13}) were chosen as the surfactant molecules. The lyotropic mixtures, which were composed of KC_x /potassium sulfate (K_2SO_4)/decanol (DeOH)/water/brucine, where brucine is a chiral dopant molecule, were studied in the frame of the present work. Partial phase diagrams were constructed to show how the surfactant alkyl chain affects the phase topologies in the phase diagrams. It was observed that while the longer the surfactant alkyl chain favors the formation of the larger discotic cholesteric, Ch_D , phase domain, the cholesteric biaxial, Ch_B , and calamitic discotic, Ch_C , regions expense. The phase transitions from the uniaxial cholesteric phases to biaxial cholesteric phase were determined from polarising optical microscopy measurements and it was shown that the Ch_D -to- Ch_B and Ch_B -to- Ch_C phase transitions shifted to lower temperatures.

KEYWORDS: Lyotropic cholesteric liquid crystals, uniaxial phases, biaxial phases, phase transitions, surfactant, potassium alkanoates, polarising optical microscopy.

ÖZET

LİYOTROPİK KARIŞIMLARDA SÜRFAKTANT ALKİL ZİNCİRİ UZUNLUĞUNUN TEK EKSENLİ-ÇİFT EKSENLİ KOLESTERİK FAZ GEÇİŞLERİ ÜZERİNE ETKİSİ

YÜKSEK LİSANS TEZİ

SEDA UYANIK

BOLU ABANT İZZET BAYSAL ÜNİVERSİTESİ

FEN BİLİMLERİ ENSTİTÜSÜ

KİMYA ANABİLİM DALI

(TEZ DANIŞMANI: DOÇ. DR. EROL AKPINAR)

BOLU, HAZİRAN - 2019

Bu çalışmada, kolesterik faz veren bazı sürfaktant temelli karışımlar, sürfaktant alkil zinciri uzunluğunun (a) tek eksenli-çift eksenli faz geçişleri ve (b) farklı kolesterik fazların stabilizasyonu üzerine etkisinin incelenmesi için hazırlanmıştır. Potasyum alkanoatlar, KC_x (potasyum undekanoat, KC_{11} ; potasyum dodekanoat, KC_{12} ; potasyum tridekanoat, KC_{13}) sürfaktant moleküller olarak seçilmiştir. Bu çalışma kapsamında, kiral konuk molekül brusin içeren KC_x /potasyum sülfat (K_2SO_4)/dekanol (DeOH)/su/brusin liyotropik karışımları ile çalışılmıştır. Faz diyagramlarında sürfaktant alkil zinciri uzunluğunun faz topolojilerini nasıl etkilediklerini göstermek için kısmi faz diyagramları çıkarılmıştır. Daha uzun alkil zincirinin daha geniş diskotik kolesterik faz (Ch_D) bölgesinin oluşmasını öncülendiği, kalamitik kolesterik (Ch_C) ve çift eksenli kolesterik (Ch_B) faz bölgelerinin ise azaldığı gözlemlenmiştir. Tek eksenli fazlardan çift eksenli faza geçişler polarize optik mikroskopisi ölçümlerinden belirlenmiştir ve Ch_D - Ch_B ile Ch_B - Ch_C faz geçişlerinin daha düşük sıcaklıklara kaydığı gösterilmiştir.

ANAHTAR KELİMELELER: Liyotropik Kolesterik Sıvı Kristaller, Tek Eksenli Fazlar Çift Eksenli Fazlar, Faz Geçişleri, Yüzey Aktif Madde, Potasyum Alkonatlar, Polarize Optik Mikroskopisi

TABLE OF CONTENTS

ABSTRACT	v
ÖZET.....	vi
TABLE OF CONTENTS.....	vii
LIST OF FIGURES	viii
LIST OF TABLES	xi
LIST OF ABBREVIATIONS AND SYMBOLS	xii
1. INTRODUCTION	1
1.1 Thermotropic Liquid Crystals	3
1.2 Lyotropic Liquid Crystals: Micellization.....	5
1.3 Lyotropic Systems.....	8
1.3.1 Lyotropic Nematic Phases	10
1.3.2 Characterization of Lyotropic Nematic Phases	12
1.3.3 Optical Features of Lyotropic Nematic Phases	13
1.3.4 Magnetic Features of Lyotropic Nematic Phases	15
1.3.5 Lyotropic Cholesteric Phases	17
2. AIM AND SCOPE OF THE STUDY	20
3. MATERIALS AND METHOD	22
3.1 Materials.....	22
3.2 Preparation of Lyotropic Liquid Crystal Samples	24
3.3 Polarizing Optical Microscopy Measurements	24
4. RESULT AND DISCUSSION.....	26
5. CONCLUSIONS.....	41
6. REFERENCES	42
7. CURRICULUM VITAE	49

LIST OF FIGURES

	<u>Page</u>
Figure 1.1. Molecular arrangements of molecules in three different states of matter.....	2
Figure 1.2. Schematic representation of the alignment of a single molecule with respect to the phase director in a liquid crystal material.....	3
Figure 1.3. Change of order parameter of a liquid crystal material with temperature.....	3
Figure 1.4. Types of thermotropic liquid crystals.	5
Figure 1.5. Molecular structures of (a) anionic, sodium dodecyl sulfate, (b)cationic, cetyltrimethylammonium Bromide, (c) non-ionic, polyoxyethylene-4-lauryl ether, and (d) zwitterionic, lecithin.....	6
Figure 1.6. The cross-section of a spherical micelle. While open-circles represent the surfactant heads, which are in contact with water molecules, the hydrophobic tails in the micelle core are shown by zigzag lines.....	7
Figure 1.7. Design of aggregation of the surfactant molecules in the micelles, depending on the packing parameters (J. Israelachvili, 1985).....	7
Figure 1.8. Structure of lamellar LLC phase.....	9
Figure 1.9. Structure of hexagonal LLC phase.	9
Figure 1.10. (a) Reversed Micellar Cubic of Fd3m, (b) Reversed Bicontinuous Cubic (Im3m), (c) Reversed Bicontinuous Cubic (Pn3m), (d) Reversed Bicontinuous Cubic (Ia3d).	10
Figure 1.11. (a) Orientations of cylindrical-like micelles in the nematic Type I or N _C phase, whose phase director is parallel to magnetic field direction. (b) In the case of the nematic Type II or N _D phase, the local directors of the disc-like micelles are parallel to the phase director but perpendicular to the magnetic field direction. The local director of the micelles is showed by the black dashed-lines.	11
Figure 1.12. Uniaxial (a) negative and (b) positive indicatrices.	11
Figure 1.13. (a) Three two-fold symmetry axes of a biaxial nematic phase and (b) a biaxial indicatrix with $n_1 \neq n_2 \neq n_3$	12
Figure 1.14. POM textures of lyotropic (a) N _D , (c) N _B (near the N _D -N _B phase transition), (e) N _B (near the N _B -N _C phase transition), and (g) N _C . Uniformly well-aligned textures of (b) N _D , (d) N _B , (f) N _B , (h) N _C	13
Figure 1.15. Homeotropic and planar alignment of the micelles in the nematic phases.	13
Figure 1.16. (a) The conoscopic investigations of well-aligned textures of uniaxial nematic phases, which show characteristic cross dark brushes. An interference figure, i.e. cross dark brushes (Maltese cross), indicates a perfect alignment of the optical axis of a nematic phase. Interference colors of nematic phases for (b) $\Delta n > 0$ and (c) $\Delta n < 0$ as a $\frac{1}{4} \lambda$ retardation plate is inserted in the light path of the polarizing light microscope. Blue arrows represent the direction of the plate.	14
Figure 1.17. Biaxial positive indicatrix (a) and biaxial negative indicatrix (b) (Wahlstrom EE, 1969; Stoiber RE, Morse SA, 1994). OA: optical axis or director; CS: circular section; Bxa: acute bisectrix; Bxo: Obtuse bisectrix (Boden et.al., 1979).	15

Figure 1.18. POM conoscopic images for (a) positive N_B and (b) negative N_B (Braga WS, 2013). (c) Laboratory frame axis (Santoro, 2006; Galerne 1983). OA represents the position of the optical axes and the dotted-line shows the lines in which the plane formed by the optical axes cut the plane of the figure (Boden et.al., 1979).....	15
Figure 1.19. The orientation of the local directors (m) of the micelles along the helix axis which is parallel to the z -axis. The micelles are assumed to have an orthorhombic symmetry as proposed by the “Intrinsically Biaxial Micelles, IBM” model of the lyotropic nematic phases (Neto et al., 1985). This model was confirmed by several experimental studies (Y. Hendrikx et al, 1986; A. M. Figueiredo Neto, 1985; Y. Galerne, 1987), considering the theoretical predictions (Galerne et al., 1987).....	18
Figure 1.20. (a) Non-aligned “fingerprint texture” and (b) well-aligned “spaghetti-like texture” of cholesteric phases.....	19
Figure 1.21. The POM textures of well-aligned (a) Ch_D , (b) Ch_B and (c) Ch_C phases, respectively.....	19
Figure 3.1. Scheme of the synthesis of surfactants KC11, KC12 and KC13.....	23
Figure 3.2. FT-IR spectrum of KC11.....	23
Figure 3.3. FT-IR spectrum of KC12.....	23
Figure 3.4. FT-IR spectrum of KC13.....	24
Figure 4.1. POM textures of the sample s1: (a) 30.00°C, Ch_D ; (b) 21.60°C, Ch_B ; (c) 18.50°C, Ch_B ; (d) 16.50°C, Ch_B ; (e) 15.00°C, Ch_B ; (f) 14.00°C, Ch_C . The sample was aligned in the magnetic field during 16 h to obtain well-aligned Ch_D phase. The sample thickness is 0.2 mm, and the magnification of the objective is 10x.	28
Figure 4.2. POM textures of the sample s2: (a) 30.00°C, Ch_D ; (b) 22.50°C, Ch_B ; (c) 21.50°C, Ch_B ; (d) 19.50°C, Ch_B ; (e) 18.50°C, Ch_B ; (f) 18.00°C, Ch_C . The sample was aligned in the magnetic field during 12 h to obtain well-aligned Ch_D phase. The sample thickness is 0.2 mm, and the magnification of the objective is 10x.	29
Figure 4.3. POM textures of the sample s3: (a) 30.00°C, Ch_D ; (b) 24.10°C, Ch_B ; (c) 23.71°C, Ch_B ; (d) 22.66°C, Ch_B ; (e) 21.66°C, Ch_B (at the Ch_B - Ch_C transition); (f) 21.16°C, Ch_C . The sample was aligned in the magnetic field during 13 h to obtain well-aligned Ch_D phase. The sample thickness is 0.2 mm, and the magnification of the objective is 10x.....	30
Figure 4.4 POM textures of the sample s4: (a) 30.00°C, Ch_D ; (b) 25.99°C, Ch_B ; (c) 25.87°C, Ch_B ; (d) 25.62°C, Ch_B ; (e) 24.50°C, Ch_C ; (f) 20.00°C, Ch_C . The sample was aligned in the magnetic field during 12 h to obtain well-aligned Ch_D phase. The sample thickness is 0.2 mm, and the magnification of the objective is 10x.	31
Figure 4.5. POM textures of the sample s5: (a) 30.00°C, Ch_D ; (b) 28.04°C, Ch_B (near the Ch_D - Ch_B transition); (c) 27.84°C, Ch_B (at the Ch_B - Ch_C transition); (d) 27.74°C, Ch_C ; (e) 20.00°C, Ch_C ; (f) 10.00°C, Ch_C . The sample was aligned in the magnetic field during 12 h to obtain well-aligned Ch_D phase. The sample thickness is 0.2 mm, and the magnification of the objective is 10x.	32

Figure 4.6. POM textures of the sample s6: (a) 30.00°C, Ch _D ; (b) 19.99°C, Ch _B (near the Ch _D -Ch _B transition); (c) 18.00°C, Ch _B ; (d) 15.00°C, Ch _B ; (e) 08.00°C, Ch _B (near the Ch _B -Ch _C transition); (f) 07.50°C, Ch _C . The sample was aligned in the magnetic field during 10 h to obtain well-aligned Ch _D phase. The sample thickness is 0.2 mm, and the magnification of the objective is 10x.	33
Figure 4.7. POM textures of the sample s7: (a) 30.00°C, Ch _D ; (b) 19.01°C, Ch _B (near the Ch _D -Ch _B transition); (c) 18.00°C, Ch _B ; (d) 13.50°C, Ch _B ; (e) 06.00°C, two-phase region; (f) 05.50°C, crystalline- or gel-like phase. The sample was aligned in the magnetic field during 10 h to obtain well-aligned Ch _D phase. The sample thickness is 0.2 mm, and the magnification of the objective is 10x.	34
Figure 4.8. POM textures of the sample s8: (a) 30.00°C, Ch _D ; (b) 18.10°C, Ch _B (near the Ch _D -Ch _B transition); (c) 17.20°C, Ch _B ; (d) 12.70°C, Ch _B ; (e) 07.20°C, Ch _B (near the Ch _B -two-phase transition); (f) 05.00°C, two-phase region;. The sample was aligned in the magnetic field during 12 h to obtain well-aligned Ch _D phase. The sample thickness is 0.2 mm, and the magnification of the objective is 10x.	35
Figure 4.9. POM textures of the sample s9: (a) 30.00°C, Ch _D ; (b) 16.94°C, Ch _B (near the Ch _D -Ch _B transition); (c) 13.50°C, Ch _B ; (d) 09.00°C, Ch _B ; (e) 06.00°C, Ch _B (near the Ch _B -two-phase transition); (f) 05.50°C, two-phase region; the sample was aligned in the magnetic field during 13 h to obtain well-aligned Ch _D phase. The sample thickness is 0.2 mm, and the magnification of the objective is 10x.	36
Figure 4.10. The partial phase diagram of the KC11/KC12 binary surfactant system as a function of the increase in the KC11 concentration in the mixtures. 2P: two-phase region.	38
Figure 4.11. The partial phase diagram of the KC12/KC13 binary surfactant system as a function of the increase in the KC13 concentration in the mixtures. 2P: two-phase region.	38
Figure 4.12. Combining the phase transition temperatures of the KC11/KC12 mixtures with those of the KC12/KC13 mixtures. The zero point, which is shown by a vertical dashed-line, corresponds to the sample s1, i.e. a single surfactant system (KC12). To the left from the zero point, the concentration of the KC11 (X_{KC11}) increases in the mixtures of the KC11/KC12. By the same way, to the right from the zero point, the concentration of the KC13 (X_{KC13}) increases in the mixtures of the KC12/KC13. In this partial phase diagram, the 2P-regions observed in the Figure 4.10 and 4.11 were ignored by starting the y-axis from 7.00°C.	39
Figure 4.13. Combining the biaxial phase region of the KC11/KC12 mixtures with those of the KC12/ KC13 mixtures. The vertical dashed line corresponds to a single surfactant system (KC12). While the concentration of the KC11 increases in the mixtures of the KC11/KC12 from s1 to s5, the concentration of the KC13 increases in the mixtures of the KC12/ KC13 from s1 to s6.	40

LIST OF TABLES

	<u>Page</u>
Table 4.1. Lyotropic mixture compositions in mole % for KC11/KC12 binary system.....	26
Table 4.2. Lyotropic mixture compositions in mole % for KC12/KC13 binary system.....	26
Table 4.3. The cholesteric to cholesteric phase transitions for KC11/KC12 binary system.....	37
Table 4.4. The cholesteric to cholesteric phase transitions for KC12/KC13 binary system.....	37



LIST OF ABBREVIATIONS AND SYMBOLS

TLCs	: Thermotropic liquid crystals
LLCs	: Lyotropic liquid crystals
Ch	: Cholesteric phase
ChB	: Cholesteric biaxial phase
ChC	: Cholesteric calamitic phase
ChD	: Cholesteric discotic phase
CMC	: Critical micelle concentration
$\Delta G^{\circ}_{\text{mic}}$: The standard Gibbs free energy of the Micellization
$\Delta H^{\circ}_{\text{mic}}$: The standard enthalpy of the Micellization
$\Delta S^{\circ}_{\text{mic}}$: The standard entropy of the Micellization
H	: Hexagonal phase
Htp	: Helical twisting power
I	: Cubic phase
L	: Lamellar phase
N	: Nematic phase
NB	: Biaxial nematic phase
NC	: Calamitic nematic phase
ND	: Discotic nematic phase
P	: Pitch
X	: Mole fraction
α	: The degree of counterion ionization
β	: The degree of counterion binding to micelle
$\Delta n/\delta n$: Birefringences
η/η_0	: Relative viscosity
POM	: Polarizing Optical Microscope,

ACKNOWLEDGEMENTS

The author wishes to express his deepest gratitude to his supervisor Assoc. Prof. Dr. Erol AKPINAR for their guidance, advice, criticism, encouragements and insight throughout the research.

The author would also like to thank Assoc. Prof. Dr. Öznur DEMİR ORDU for her suggestions and comments.

The technical assistance of Mrs. Nazlı UYGUR and Mrs. Esra ŞAHİN are gratefully acknowledged.

This study was supported by The Scientific and Technological Research Council of Turkey (TUBITAK), Grant No: 117Z783.

1. INTRODUCTION

Liquid crystals were discovered for the first time in 1888 by Friedrich Reinitzer, an Austrian botanist and chemist (Reinitzer F., 1989). They are anisotropic fluids that are thermodynamically located between anisotropic solids and isotropic liquids. From this respect, liquid crystals can be regarded as the fourth state of matter presenting some degree of fluidity (like liquids) and exhibiting long-range order similar to solids. They owe their anisotropy to rod-shaped (rarely disc-shaped) molecules that have a relatively rigid, polarizable middle part and flexible end groups. The most basic and lean definition of liquid crystals might like, partially ordered systems without a rigid, long-range structure (Ranjesh A. et al, 2019). The study of these materials covers a wide area: chemical structure, physical properties and technical applications. Because of their easy responses to externally applied electric, magnetic, optical and surface fields, liquid crystals are of greatest potential for scientific and technological applications (Singh, 2002).

Description of a structure of liquid crystal would be like neither long chain nor short organic molecules and they tend to be elongated as well (Maier, W., Saupe, A. 1958). Their behaviors depend on the temperature and they show two different states of matter. At low temperature, they behave like a solid and at high temperature their coordinated structure collapse therefore anisotropic state.

Considering a thermodynamic stable system, it prefers to reach a state which requires maximum entropy and minimum Gibbs energy (H. Kunieda, K, Shinoda, 1978). Since the entropy is related to the extent of order or disorder in a system, the solid state is described with the lowest entropy and the highest order in terms of the molecular arrangement. The latter indicates that molecules have certain position in a 3D dimensional structure of a crystal and molecules oriented along a certain direction (Figure 1.1a). Because of this, the solid state of a material represents both positional and directional (or orientational) orders. On the contrary, molecules are distributed randomly in a liquid state which means that there exist no positional and

orientational orders (Figure 1.1c). In the case of a liquid crystal state, there exist some degree of both orientational and positional orders, Figure 1.1b.

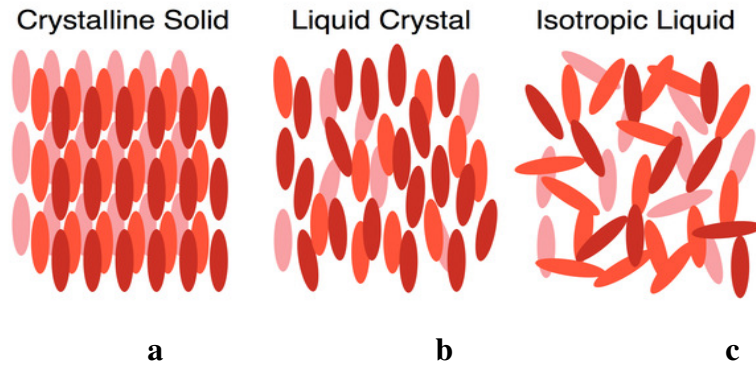


Figure 1.1. Molecular arrangements of molecules in three different states of matter.

As seen from Figure 1.1, the degree of order is different in three states of the matter and it decreases going from solid to isotropic state. The degree of order of a liquid crystal material is given by “order parameter, S” (de Gennes P. G. and Prost J. 1993; Chandrasekhar S. 1977)

$$S = \frac{1}{2} (3\cos^2\theta - 1) \quad (1.1)$$

where θ is the angle between the long molecular axis and the preferred direction of the alignment of the molecules, the so-called “director or optical axis, \vec{n} ” in a liquid crystal material, Figure 1.2. The order parameter can take values between zero and one. While $S=0$ for completely disordered liquid crystal system (similar to isotropic liquid), $S=1$ corresponds to the completely ordered one, like perfectly positioned molecules of a solid material. The change in the order parameter is given in Figure 1.3, i.e. it decreases as the temperature is raised. Sudden change observed on the curve is called the transition temperature from a liquid crystal phase to the isotropic phase, T_{LI} .

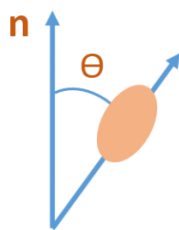


Figure 1.2. Schematic representation of the alignment of a single molecule with respect to the phase director in a liquid crystal material.

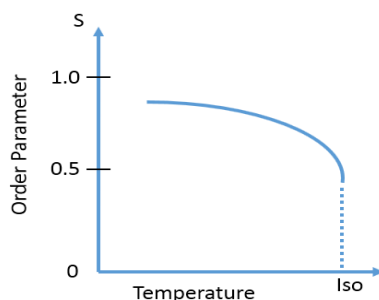


Figure 1.3. Change of order parameter of a liquid crystal material with temperature.

Liquid crystals are mainly divided into two basic classes, being “thermotropic, TLC” and “lyotropic, LLC” liquid crystals. The structural units of TLCs and LLCs are molecules and micelles, respectively. While different TLC phases are obtained by changing temperature, both temperature and relative concentrations of the constituents of LLC mixtures cause the formation of different LLC phases. Of particular interest of this thesis is the LLCs, indeed lyotropic uniaxial and biaxial cholesteric phases, but not the TLCs. Thus, we will give some short information on the TLCs in the further parts.

1.1 Thermotropic Liquid Crystals

TLCs are single component systems, i.e. their molecules self-assemble to give ordered phases in the absence of any other component. They are important materials in technological applications such as liquid crystal displays (LCD) (George H. Heilmeyer and Joel E. Goldmacher, 1968), light valves (White D.L., Feldman M., 1970), biosensors (Emmanuel I. Iwuoha, Malcolm R. Smyth, 2002), temperature and pressure sensors (G. M. Zharkova et al., 2018), etc. TLCs are formed at a certain

temperature range. TLC materials are in the form of solid crystals at low temperatures and transform into a liquid crystal structure (mesophase) at relatively high temperatures. For a material to exhibit mesomorphic properties, two conditions must be fulfilled: the molecules must be rod-shaped or disc-shaped and geometrically anisotropic (Palffy-Muhoray et al., 1985). The molecules of TLCs often have higher (lower) dipole moments at the center or near the center (at the edges) (Yu. K. Kornienko and A. P. Fedchuk, 1997).

The interaction forces between molecules in liquid crystals are examined in three ways (Keesom, W.H, 1913; Debye, P., 1920; London, F., Z 1930):

1. Dipole-dipole interactions between continuous molecule dipoles.
2. Inductive dipole interactions; these interactions depend on the inter polarizations of the molecules and the permanent dipole moments. The forces arise from the interactions between polar-polar molecules and polar-nonpolar molecules.
3. Dispersion forces, the most common type of intermolecular interaction forces; it is possible to regard these forces as forces between the instantaneous dipole moments that occur with combinations of electron orbits.

If an isotropic liquid is converted into a TLC structure, the attractive forces between the dipoles cause the molecules to be arranged close to and parallel to each other. In this case, the share of the dipole-dipole component of the dispersion interaction increases (Israelachvili, J.N., 1992).

Thermotropic liquid crystals are mainly divided into three types: smectics, nematics and cholesteric. The molecular arrangements in these phases are given in Figure 1.4. In a nematic TLC phase, the molecules exhibit long-range orientational order, but not positional one, Figure 1.4a, (Yeh and Gu, 1999). Two types of smectic mesophases are defined as smectic A and smectic C. In the smectic phases, there exist both positional and orientational order, (Yeh and Gu, 1999). In the phase diagrams, in general, the smectic phases are observed at lower temperatures with respect to the nematic ones. The main feature of the smectic phases is that the molecules stack into layers where orientation of molecules is responsible for the type

of the smectic phase (Neto and Salinas, 2005). In the smectic A phase, the orientations of the molecules are perpendicular to the layers, and parallel to both the layers normal (z) and phase director (n), Fig. 1.4b. In the smectic C phase, the molecules are tilted with respect to the layer normal and the director points at an angle to the layer normal, Fig. 1.4c. The last type of the TLC phase is a cholesteric phase. The molecules possess ‘chirality’ and their chiralities are transferred to the whole phase to form the cholesteric phase. The characteristic property of the cholesteric phase is that the molecules are arranged to form helical structure, Figure 1.4d, where the local director of the molecule is twisted along a certain axis, the so-called ‘helix axis’. The cholesteric TLC phase can be obtained either the direct use of a chiral molecule, which gives TLCs, or doping nematic phase with a chiral molecule.

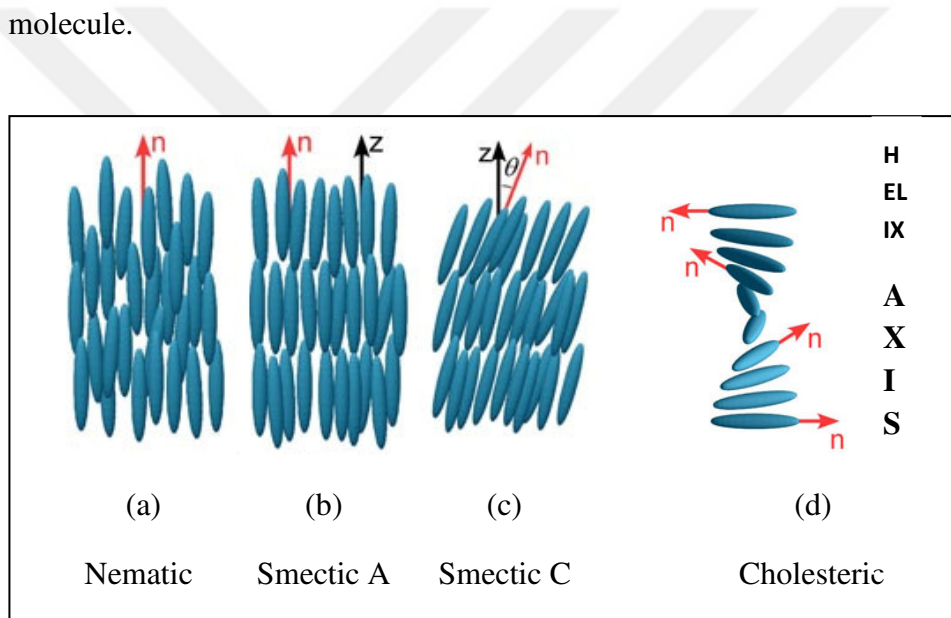


Figure 1.4. Types of thermotropic liquid crystals.

1.2 Lyotropic Liquid Crystals: Micellization

The dissolution of certain organic substances (amphiphiles or surfactants) in polar or non-polar solvents causes the formation of LLC systems. Unlike TLCs, LLC systems have mesomorphic properties not only at certain temperature ranges but also at a certain concentration range, i.e. temperature and concentration control the formation of different LLC structures (Signh, 2002; Neto and Salinas, 2005).

LLCs are thought to be as the dispersion of their structural units ‘micelles’ in a solvent (mostly water). The surfactant molecules consist of two parts in terms of the interactions with the solvents, polar or ionic head and non-polar tail, and form the micelles in different shapes. Their polar heads determine the classification of the surfactants as anionic, cationic, non-ionic or zwitterionic, Figure 1.5 (Zhou & Zhao, 2009).

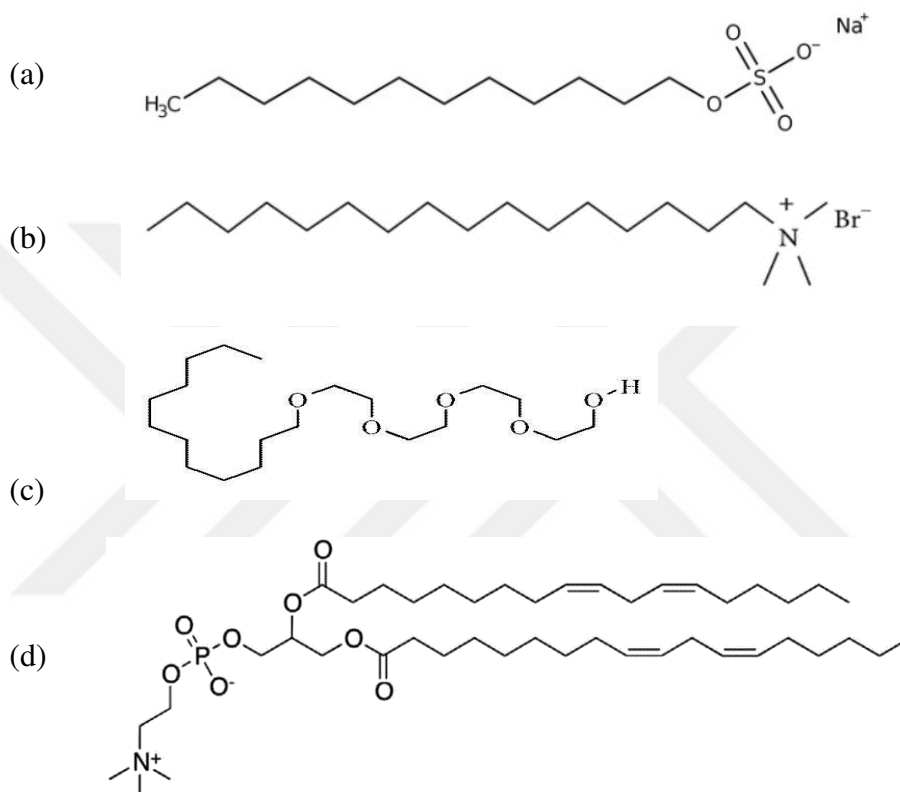


Figure 1.5. Molecular structures of (a) anionic, sodium dodecyl sulfate, (b) cationic, cetyltrimethylammonium Bromide, (c) non-ionic, polyoxyethylene-4-lauryl ether, and (d) zwitterionic, lecithin.

At very low concentrations of the surfactants in water, there is an equilibrium between the surfactant monomers existing at the water/air interface and in the bulk. When the concentration increases, the surface of the solution is saturated by the surfactant molecules and then, by the further addition of the surfactants, the micelles are formed. The minimum concentration at which surfactant molecules aggregate to form the micelles is called ‘critical micelle concentration, cmc’. At or very near the cmc, the micelles are almost spherical in shape, Figure 1.6, and the micelle shape may change above the cmc, depending on the packing geometry of the surfactant

molecules in the micelles. Indeed, it may be said that the micelle shape is related to the ‘critical packing parameter’, Figure 1.7.

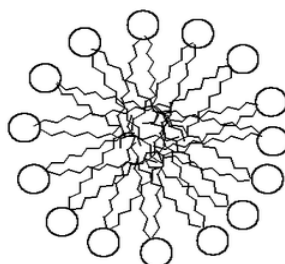


Figure 1.6. The cross-section of a spherical micelle. While open-circles represent the surfactant heads, which are in contact with water molecules, the hydrophobic tails in the micelle core are shown by zigzag lines.

Lipid	Critical packing parameter $v/a_0 \ell_c$	Critical packing shape	Structures formed
Single-chained lipids (surfactants) with large head-group areas: <i>SDS in low salt</i>	$< 1/3$	Cone 	Spherical micelles
Single-chained lipids with small head-group areas: <i>SDS and CTAB in high salt, nonionics</i>	$1/3-1/2$	Truncated cone 	Cylindrical micelles
Double-chained lipids with large head-group areas, fluid chains: <i>Phosphatidyl choline (lecithin), Phosphatidyl serine, Phosphatidyl glycerol, Phosphatidyl inositol, Phosphatidic acid, sphingomyelin, DGDG^a, dihexadecyl phosphate, dialkyl dimethyl ammonium salts</i>	$1/2-1$	Truncated cone 	Flexible bilayers, vesicles
Double-chained lipids with small head-group areas, anionic lipids in high salt, saturated frozen chains: <i>phosphatidyl ethanolamine, phosphatidyl serine + Ca²⁺</i>	~ 1	Cylinder 	Planar bilayers
Double-chained lipids with small head-group areas, nonionic lipids, poly (<i>cis</i>) unsaturated chains, high <i>T</i> : <i>unsat. phosphatidyl ethanolamine, cardiolipin + Ca²⁺, phosphatidic acid + Ca²⁺, cholesterol, MGDG^b</i>	> 1	Inverted truncated cone or wedge 	Inverted micelles

Figure 1.7. Design of aggregation of the surfactant molecules in the micelles, depending on the packing parameters (J. Israelachvili, 1985)

In the structure of a micelle, its outer surface is composed of the hydrophilic parts of the amphiphilic molecules, while its inner part (micelle core) consists of hydrophobic parts. The formation of the micelles in such a way that no water passes through the interior is due to the reduction of accumulated free energy. There is a critical temperature, so-called “Krafft temperature”, for each amphiphile. Micelles cannot be present below this temperature in micellar systems. Some parameters affect the micelle formation. For instance, increasing the length of the alkyl chains in the hydrophobic portions of the amphiphiles allows the CMC to shift to lower concentrations (Dominguez et al., 1997; Garcia Mateos et al., 1990; Chattopadhyay and Erwin London, 1984; Lin et al., 1999; Salem et al., 2016). Furthermore, the addition of an electrolyte (salt) is favored the micelle formation, i.e. the cmc decreases (Hamley, 1998).

The formation of micelles is a free process and the Gibbs energy of micellization is negative, $\Delta_{\text{mic}}G < 0$ (Zana, R., 1998). The most important contribution to the $\Delta_{\text{mic}}G$ is provided by $T\Delta_{\text{mic}}S$ (C. Carnero Ruiz, 1999). Enthalpy change of the micellization, $\Delta_{\text{mic}}H$, provides small contribution to the $\Delta_{\text{mic}}G$. This is the consequences of settling the hydrophobic tails of the amphiphilic molecules into the micelles and contacting the hydrophilic heads with the water (Zajac, J. et al, 1997). The formation of the micelles breaks down the structure of the water and thus increases the entropy of the micellar system ($\Delta S > 0$), (H. Kunieda, K, Shinoda, 1978).

If the amount of the surfactant molecules is enough, the isotropic micellar solutions may be turned into the different lyotropic structures of phases. In the latter case, the micelles get more anisometric. In the following part, information on the lyotropic structures is given.

1.3 Lyotropic Systems

Depending on the packing of the surfactants in the micelles, which affects the micelle shape and the organization of the micelles in the lyotropic mixtures, the

different LLC structures are formed. Lamellar, hexagonal, cubic (discontinuous and bicontinuous), nematic and cholesteric (or chiral nematic) phases are well-known LLC structures. The surfactant molecules are packed in the infinitively large bilayers of the lamellar LLC phase (L), Figure 1.8. In the L phase, it can be thought that the water molecules are sandwiched between the bilayers. The hexagonal phase (H) consists of infinitively long rod-shaped (cylindrical) micelles, which are organized into a hexagonal arrangement, Figure 1.9. Both the L and H phases are obtained in high concentration of the surfactant molecules. Since the former one exhibits less viscosity, the latter one is described by its high viscosity.

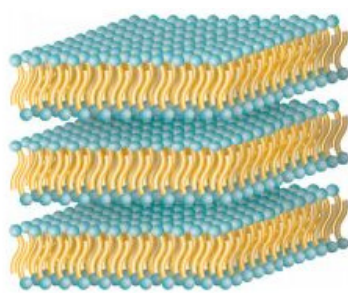


Figure 1.8. Structure of lamellar LLC phase.

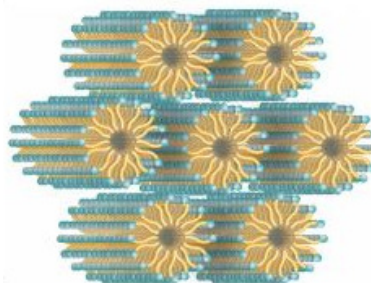


Figure 1.9. Structure of hexagonal LLC phase.

In the cubic phases, the micelles are arranged into a discontinuous or bicontinuous arrangement. The cubic phases are more viscous if they are compared to the H ones. Some cubic phase structures are given in Figure 1.10 (Yiming Huang and Shuangying Gu, 2018).

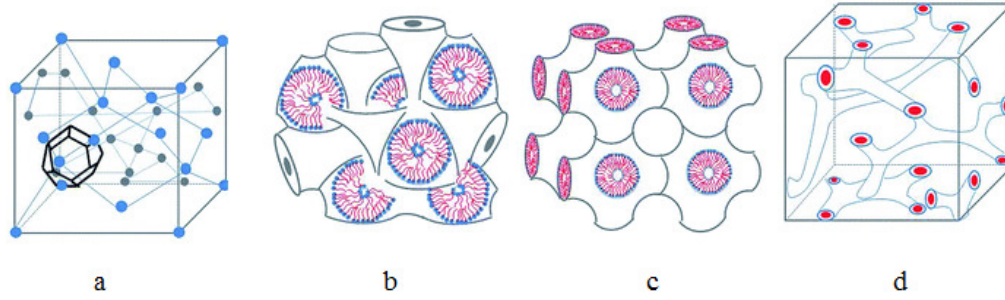


Figure 1.10. (a) Reversed Micellar Cubic of $Fd3m$, (b) Reversed Bicontinuous Cubic ($Im3m$), (c) Reversed Bicontinuous Cubic ($Pn3m$), (d) Reversed Bicontinuous Cubic ($Ia3d$).

This thesis is mainly related to the lyotropic cholesteric phases. Thus, in the further parts, we will give detailed information on them. However, it would be better if we give information on the lyotropic nematic phases because the lyotropic cholesteric phases are often obtained from doping the lyotropic nematics with chiral guest molecules (dopants).

1.3.1 Lyotropic Nematic Phases

Since the discovery of first lyotropic mixture presenting nematic phase towards the end of the 1960s (Lawson and Flautt, 1967; Rosevear, 1968), the scientists paid their attentions to develop their properties. In these early studies, the two types of nematic phases were identified: Type I and Type II (Kleman and Lavrentovich, 2006; Senyuk et.al., 2011; Serra, 2016). This classification was based on the orientation of the phase director (optical axis, \vec{n} , which represents the preferred alignment of the individual micelles with their local directors) in the presence of the external magnetic field. While the director of the Type I phase aligns parallel to the magnetic field direction, \vec{H} , that of the Type II is in the perpendicular direction to the \vec{H} (Alcantara MR et al., 1984; Acimis M, Reeves LW, 1980). Notice that the micelle shapes in the Type I and Type II were assumed to be cylindrical-like and disc-like, respectively, Figure 1.11 (Neto et al., 1985; Galerne et al., 1987). Later, the researchers were classified Type I and Type II phases as calamitic nematic (N_C) and discotic nematic (N_D) phases (Photinos, P. et al., 1986)

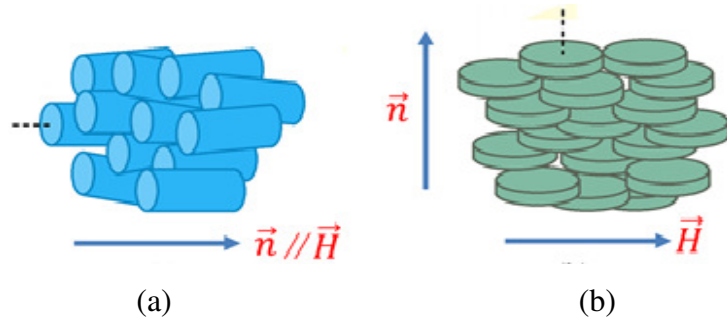


Figure 1.11. (a) Orientations of cylindrical-like micelles in the nematic Type I or N_C phase, whose phase director is parallel to magnetic field direction. (b) In the case of the nematic Type II or N_D phase, the local directors of the disc-like micelles are parallel to the phase director but perpendicular to the magnetic field direction. The local director of the micelles is showed by the black dashed-lines.

From the symmetry point of view, lyotropic nematic phases are identified as uniaxial and biaxial. The uniaxial nematic phases are the N_D and the N_C phases, with $D_{\infty h}$ symmetry (Badikov et al., 2009) and only one optical axis (director, represented by a vector \vec{n}), separately, Figure 1.11. In three dimensions, the nematic phases can be defined by three refractive indices. If the refractive index is parallel to the optical axis, $n_{||}$, which is also known as the refractive index of the extraordinary ray (n_e), is smaller than the one perpendicular to the optical axis, n_{\perp} (refractive index of the ordinary ray, n_o), and the uniaxial nematic phase may have negative birefringences ($\Delta n = n_e - n_o = n_{||} - n_{\perp} < 0$) with a uniaxial negative indicatrix, Figure 1.12a. On the contrary, it may also have positive birefringences, $\Delta n > 0$, where $n_{||} > n_{\perp}$, with a uniaxial positive indicatrix, Figure 1.12b. It is well-known in the literature that the N_D and N_C phases are described by positive and negative birefringences, respectively (M. Simoes et. al., 2019).

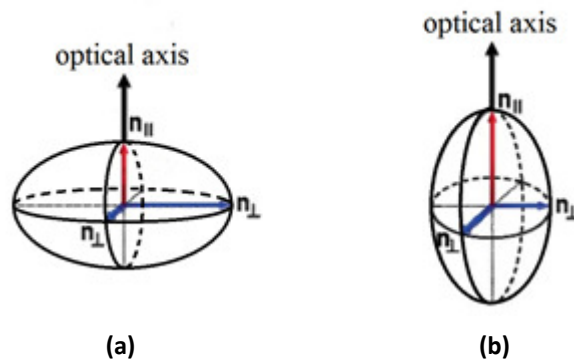


Figure 1.12. Uniaxial (a) negative and (b) positive indicatrices.

In the case of the biaxial one, N_B , there exist two optical axes with D_{2h} symmetry (Sutherland, 1996; Dimitriev et al. 2010). In addition, there are three orthogonal two-fold symmetry axes (\vec{l} , \vec{m} and \vec{n} , where $\vec{n} = \vec{l} \times \vec{m}$) in the N_B phase, Figure 1.16a. In the N_B phase, three refractive indices are not equal to each other, $n_1 \neq n_2 \neq n_3$, and the biaxial indicatrix is a completely asymmetric ellipsoid as in Figure 1.13b (M. Lehmann, 2009).

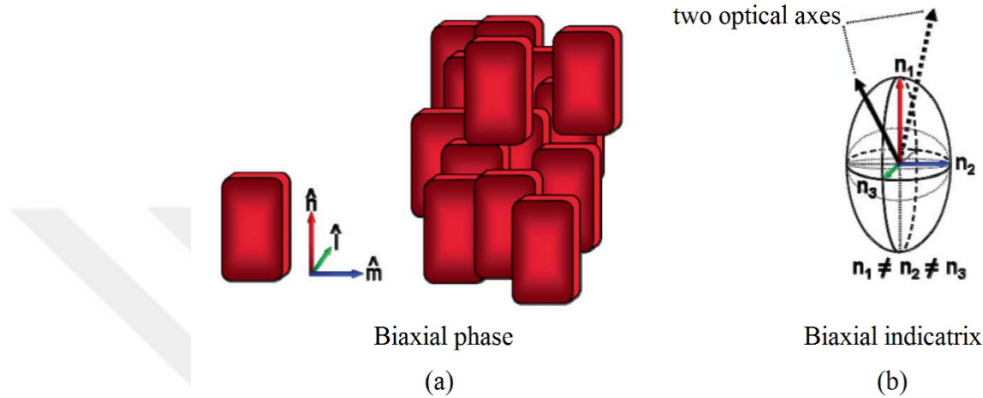


Figure 1.13. (a) Three two-fold symmetry axes of a biaxial nematic phase and (b) a biaxial indicatrix with $n_1 \neq n_2 \neq n_3$.

1.3.2 Characterization of Lyotropic Nematic Phases

Lyotropic nematic phases are characterized by a polarizing optical microscope (POM). They give characteristic ‘schlieren texture’, Figure 1.14 a, 1.14c, 1.14e and 1.14g. The nematic samples are sandwiched between two optical flat glasses or transferred into the flat capillaries. The latter one is mainly applied to the sample preparation for the POM analysis. When a nematic sample is aligned with a surface effect or in an external magnetic field, it gives homogeneous textures in three nematic phases. If the phase is N_D , the homeotropic or pseudo-isotropic texture is observed, Figure 1.14b. If the phase is N_C , the planar alignment is in question, Figure 1.14h. The homeotropic and planar alignments are given in Figure 1.15. If the phase is N_B , the well-aligned texture is similar to Figure 1.14d and f.

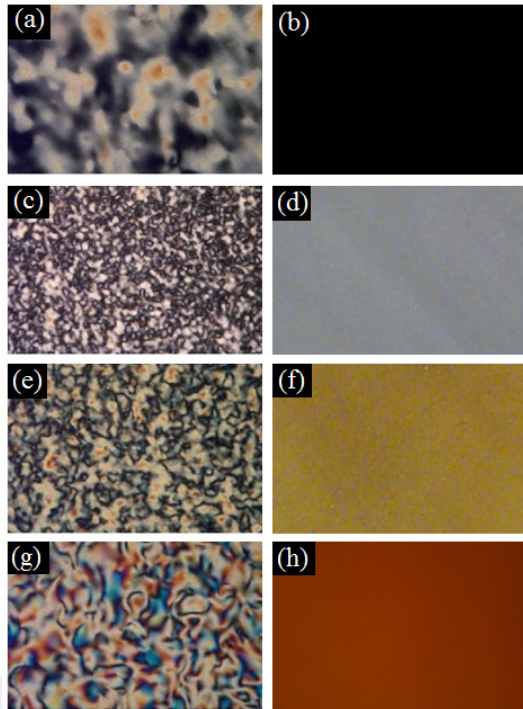


Figure 1.14. POM textures of lyotropic (a) N_D , (c) N_B (near the N_D - N_B phase transition), (e) N_B (near the N_B - N_C phase transition), and (g) N_C . Uniformly well-aligned textures of (b) N_D , (d) N_B , (f) N_B , (h) N_C .

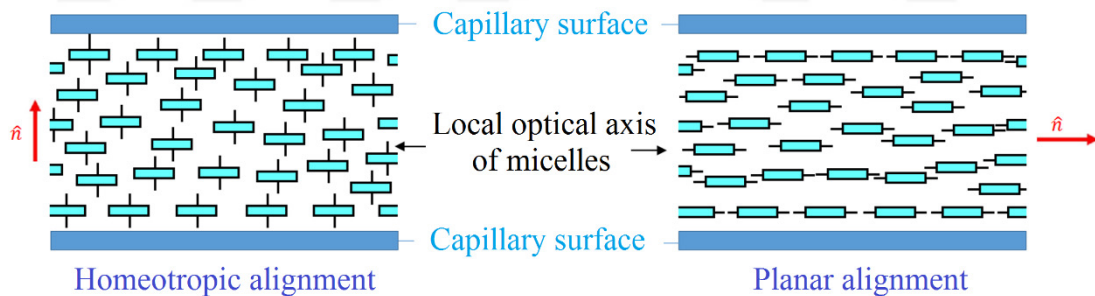


Figure 1.15. Homeotropic and planar alignment of the micelles in the nematic phases.

1.3.3 Optical Features of Lyotropic Nematic Phases

Liquid crystals are anisotropic materials similar to the solids. While a polarized light beam is passed through a lyotropic uniaxial nematic sample, two plane-polarized rays with two different refractive indices (n) appear. These rays are called ‘ordinary ray, n_o ’ and ‘extraordinary ray, n_e . Their electric vectors vibrate or

propagate in different directions with respect to the optical axis (director) of the nematic phase. The propagation direction of electric vector of the extraordinary ray is parallel to the director of the nematic phase, so n_e is also shown as $n_{//}$, i.e. $n_e=n_{//}$. On the other hand, the propagation direction of electric vector of the ordinary ray is in the perpendicular direction and $n_o=n_{\perp}$. The difference between these two refractive indices, as we mentioned before, gives an important parameter for the optical anisotropy of the nematic phases, known as ‘double refraction’ or ‘optical anisotropy’ or ‘birefringence’, $\Delta n=n_e-n_o=n_{//}-n_{\perp}$. There are three possibilities for the value of Δn . If it is zero, i.e. $n_e=n_o$, the system is isotropic. If $n_{//}>n_{\perp}$ ($n_{//}<n_{\perp}$), the optical anisotropy of the sample is greater (smaller) than zero. The N_D and N_C phases exhibit positive and negative birefringence ($\Delta n>0$ and $\Delta n<0$), respectively (de Jeu, W. H., 1980; Demus, D., et al 1998). Consequently, similar to uniaxial crystals, the uniaxial nematic phases can be divided into two classes: positive and negative. Experimentally, the sign of optical anisotropy can be easily evaluated from conoscopic investigation of well-aligned uniaxial nematic samples, Figure 1.14b and 1.14h, under the POM with Bertrand lens and $\frac{1}{4}$ retardation plate, Figure 1.16.

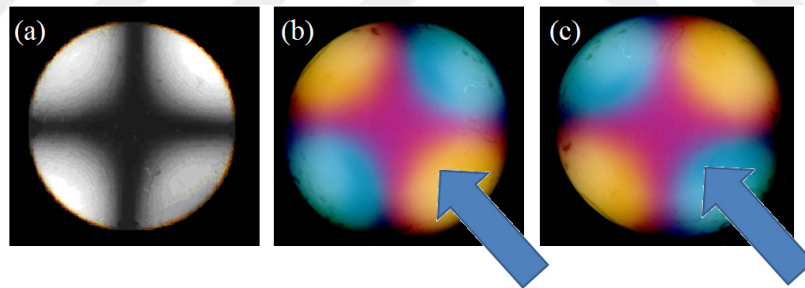


Figure 1.16. (a) The conoscopic investigations of well-aligned textures of uniaxial nematic phases, which show characteristic cross dark brushes. An interference figure, i.e. cross dark brushes (Maltese cross), indicates a perfect alignment of the optical axis of a nematic phase. Interference colors of nematic phases for (b) $\Delta n>0$ and (c) $\Delta n<0$ as a $\frac{1}{4} \lambda$ retardation plate is inserted in the light path of the polarizing light microscope. Blue arrows represent the direction of the plate.

In the case of the N_B phase, there exist three different refractive indices; n_1 , n_2 and n_3 (Figure 1.13b) with $n_1 \neq n_2 \neq n_3$. If $n_3 - n_2 > n_2 - n_1$, $\Delta n > 0$ and $n_3 - n_2 < n_2 - n_1$ indicates $\Delta n < 0$ (M. Simões et al., 2019). Thus, the biaxial nematics are classified

as positive and negative biaxial ones. The positive and negative biaxial indicatrices are given in Figure 1.17.

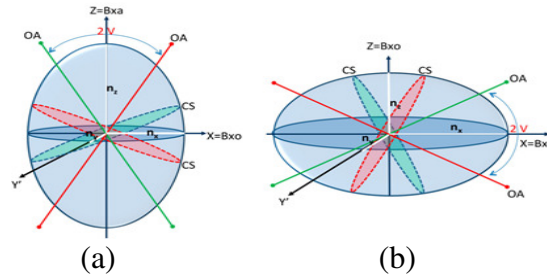


Figure 1.17. Biaxial positive indicatrix (a) and biaxial negative indicatrix (b) (Wahlstrom EE, 1969; Stoiber RE, Morse SA, 1994). OA: optical axis or director; CS: circular section; Bxa: acute bisectrix; Bxo: Obtuse bisectrix (Boden et.al., 1979).

The sign of the biaxial nematics can be determined by conoscopic measurements under the POM. Unlike the uniaxial nematic phases, the isogyres opens and there exist two optical axes, Figure 1.18, (Galerne Y, Marcerou JP, 1983; Santoro PA et al., 2006; Braga WS, 2013).

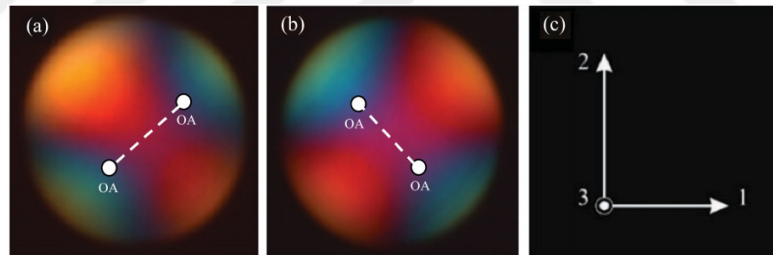


Figure 1.18. POM conoscopic images for (a) positive N_B and (b) negative N_B (Braga WS, 2013). (c) Laboratory frame axis (Santoro, 2006; Galerne 1983). OA represents the position of the optical axes and the dotted-line shows the lines in which the plane formed by the optical axes cut the plane of the figure (Boden et.al., 1979).

1.3.4 Magnetic Features of Lyotropic Nematic Phases

Liquid crystals are diamagnetic materials and they show susceptibility against the applied magnetic field (Boden et.al., 1981). Because the optical axes of the lyotropic nematic phases align differently in the magnetic field, they are also classified in terms of their diamagnetic susceptibilities. There are two possibilities for alignment of optical axes with respect to the magnetic field direction: either

parallel to the applied magnetic field, $\chi_{//}$, or in the perpendicular direction to the magnetic field, χ_{\perp} . The difference between these two components of diamagnetic susceptibilities, $\chi_{//} - \chi_{\perp}$, determines the diamagnetic susceptibility anisotropy, $\Delta\chi$, of the lyotropic nematic phases. If $\chi_{//} > \chi_{\perp}$, a lyotropic nematic phase has a positive diamagnetic susceptibility anisotropy ($\Delta\chi > 0$) and its optical axis or director aligns parallel to the direction of applied magnetic field. (Neto and Salinas, 2005). In the case of $\chi_{//} < \chi_{\perp}$, $\Delta\chi < 0$ and the optical axis is perpendicular to the magnetic field direction (Boden et.al., 1979). If $\chi_{//} = \chi_{\perp}$, the diamagnetic susceptibility anisotropy is equal to zero and the system is isotropic.

As we stated in the previous parts, the optical axes of the uniaxial N_D and N_C phases align perpendicular ($\Delta\chi < 0$) and parallel ($\Delta\chi > 0$) to the applied magnetic field, the N_D and N_C phases are labelled as N_D^- and N_C^+ , respectively. Their well-aligned textures are seen in the Figures 1.14b and 1.14h, respectively.

The biaxial nematic phases are described by the diamagnetic susceptibilities along three two-fold symmetry axes being χ_{33} , χ_{22} and χ_{11} . The diamagnetic susceptibility anisotropy of the biaxial nematics is given by:

$$\Delta\chi = \chi_{33} - \frac{\chi_{11} + \chi_{22}}{2} \quad (1.1)$$

If the largest diamagnetic susceptibility is larger than the average of the diamagnetic susceptibilities of other axes, $\Delta\chi > 0$ and the biaxial phase aligns parallel to the magnetic field direction (Quist, 1995; Melo Filho et al., 2003). Conversely, if the smallest diamagnetic susceptibility is less than the average of the diamagnetic susceptibilities of other axes, $\Delta\chi < 0$ and the biaxial phase aligns perpendicular to the magnetic field direction. Consequently, two different N_B phase regions with positive and negative diamagnetic susceptibility anisotropies, N_B^+ and N_B^- , respectively, are observed in the phase diagrams (Quist, 1995).

1.3.5 Lyotropic Cholesteric Phases

In terms of micelle shapes or symmetry, lyotropic cholesteric phases, similar to the nematic ones, are classified as discotic cholesteric (Ch_D), biaxial cholesteric (Ch_B) and calamitic cholesteric (Ch_C) phases. They have long-range orientational order and a short-range translational order. D- or L-enantiomeric forms of DL-racemic surfactants (Akpinar et al., 2001; Radley and Cattey, 1992) or doping a chiral guest agent into a nematic phase (Lee and Labes, 1984; Reis et al., 2013) can be chosen a way to prepare a mixture of the cholesteric phases. The cholesteric phases obtained by the former and latter ways are called ‘intrinsic’ and ‘induced’ cholesteric phases (Neto and Salinas, 2005). The cholesteric phases are differentiated from their nematic counterparts by the formation of the “helical structure” (Ferrarini et.al., 1999; Kuball and Türk, 1999). By the effect of the chirality of chiral molecule present in the mixture, an enantiomeric surfactant or a chiral dopant, the local director (m) of the chiralized micelle spins around a certain axis, so-called “helix axis”, to gain its original position or, in other words, to complete 2π -rotation, Figure 1.19. In the case of the lyotropic cholesteric phase, the helix axis is also optical axis or director of the phase. The cholesteric phases are characterized two important physical parameters: helical pitch (P) and helical twisting power (htp). The P corresponds to the 2π -rotation of the local director of the micelles around the helix axis (Ferrarini et.al., 1999; Kuball and Türk, 1999). The P and htp are related to one another by

$$P^{-1} = (\pm) htp.x_i \quad (1.2)$$

where P^{-1} is the reciprocal of the pitch (also known as “twist”) and x_i is the mole fraction of the L-enantiomer or chiral guest molecule in the lyotropic mixture.

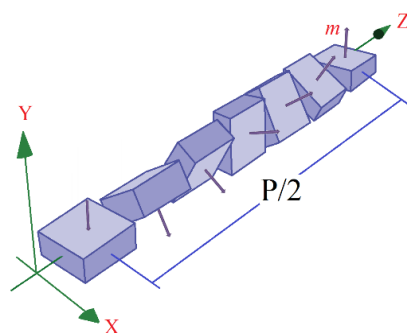


Figure 1.19. The orientation of the local directors (m) of the micelles along the helix axis which is parallel to the z -axis. The micelles are assumed to have an orthorhombic symmetry as proposed by the “Intrinsically Biaxial Micelles, IBM” model of the lyotropic nematic phases (Neto et al., 1985). This model was confirmed by several experimental studies (Y. Hendrikx et al, 1986; A. M. Figueiredo Neto, 1985; Y. Galerne, 1987), considering the theoretical predictions (Galerne et al., 1987).

Although there still exist some discussions on how the chiral molecules transfer their chiralities to the whole phase, some models were proposed to explain the chiral induction mechanisms of the lyotropic cholesteric phases. Among them, two important models were widely accepted (Radley and Saupe, 1978; Partyka and Hiltrop, 1996; Pape and Hiltrop, 1997). The first model, which is known as ‘a chiral dispersion interaction model’, assumes direct pairwise interactions between one chiral dopant present in a micelle and another one in a neighboring one. In the second model, so-called ‘a chiral sterical interaction model’, it is proposed that a non-chiral or achiral micelle of the lyotropic nematic phase is distorted to give the chiralized micelle and then the thermal movements and the collisions of the distorted or chiralized micelles lead to chirality transportation from one micelle to next micelle along the whole phase (Partyka and Hiltrop, 1996; Pape and Hiltrop, 1997). Consequently, while a macroscopic twist arises from the intermicellar interactions and intramicellar twist in the first and second models, respectively (Partyka and Hiltrop, 1996). NMR experiments showed that the second model is more acceptable with respect to the first one (Tracey, A.S. and Radley, K., 1984).

Lyotropic cholesteric phases are characterized by polarizing optical microscope. In general, they give ‘fingerprint’ and ‘spaghetti-like’ textures, Figure 1.20a. The texture in the Figure 1.21a is observed for well-aligned uniaxial Ch_D phases. In the case of the Ch_B phase, there exist two-optical axes and the incident

light moving into the Ch_B pattern is not parallel to the director in the dark regions as observed for the Ch_D phases, Figure 1.21b. In the Ch_C phases, the helix axis is parallel to the local director of the micelles and the helical structure is unwound by a magnetic field or surface effect, which leads to the disappearance of the cholesteric stripes, Figure 1.21c.

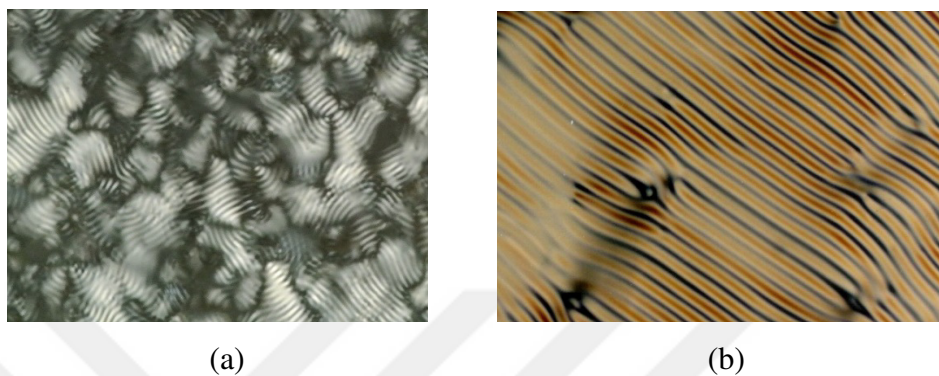


Figure 1.20. (a) Non-aligned “fingerprint texture” and (b) well-aligned “spaghetti-like texture” of cholesteric phases.

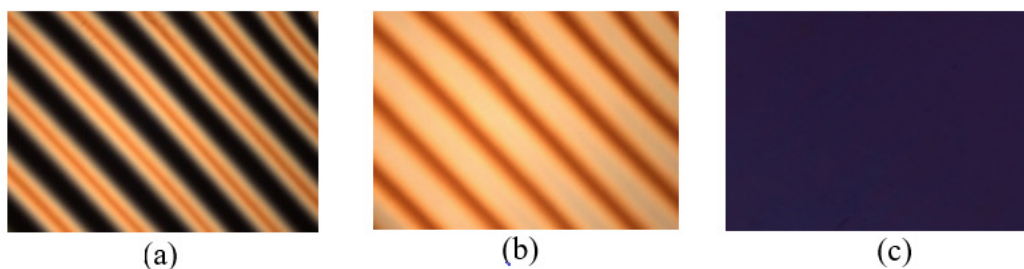


Figure 1.21. The POM textures of well-aligned (a) Ch_D , (b) Ch_B and (c) Ch_C phases, respectively.

2. AIM AND SCOPE OF THE STUDY

Lyotropic nematic and cholesteric phases are widely studied in the literature because their structural units, so-called ‘micelles’, organize in their whole structures with respect to the phase director (\vec{n}) in the presence of the magnetic field. In both phases, there exists long-range orientational order and the micelles have finite sizes. However, the cholesteric ones differ from the nematic counterparts since the former exhibit the helical structure and the helix axis is the phase director of the cholesteric phase.

In the phase diagrams, the Ch_B is located between other two uniaxial ones, Ch_D and Ch_C (Neto, A. M, 1985; Helene M., 1988; de Sant’Ana, 1992). The phase transitions between uniaxial and biaxial phases were of the subject in some studies reported in the literature. While the phase transitions from uniaxial to biaxial phases are of second order, as predicted by mean-field theory, in the case of the lyotropic nematic phases (Freiser MJ, 1970) however, the uniaxial Ch_D or Ch_C to the Ch_B phase transitions are of first order or continuous as were theoretically proposed (Brand and Pleiner, 1985) and experimentally proved (Kroin, T. et al, 1989) However, in those studies, the authors were concentrated on the describing the order of the cholesteric-to-cholesteric phase transitions, except that we showed, for the first time, the first order cholesteric-to-cholesteric phase transitions by studying the effect of alkyl chain length of long-chain alcohols on cholesteric uniaxial to cholesteric biaxial phase transitions (Reis D, et al, 2013)

The effect of the surfactant alkyl chain length on uniaxial-to-biaxial nematic phase transitions via polarising optical microscopy, laser conoscopy and small-angle x-ray scattering was reported in the literature (Akpınar E, et al, 2017). It was proved that the surfactant alkyl chain length is an important parameter (a) to stabilize different nematic phases, (b) on the birefringences of the nematic phases and (c) on the uniaxial-to-biaxial phase transitions. That study showed that the longer the surfactant alkyl chain length gives rise to the formation of the larger N_D phase

domain, expensing both N_C and N_B phase domains and shifting the uniaxial-to-biaxial phase transition temperatures. Furthermore, the micelle shape anisotropy increases as a result of the increase in the surfactant alkyl chain length by the additional $-CH_2$ group.

To the best of our knowledge, a systematic investigation of the effect of the surfactant alkyl chain length on the lyotropic cholesteric uniaxial to cholesteric biaxial phase transitions has not been reported in the literature yet. The lyotropic nematic host mixtures were composed of potassium alkanoates (KCx)/potassium sulfate (K_2SO_4)/decanol (DeOH)/water and the cholesteric phases were obtained from these mixtures by doping with the chiral dopant molecule 'brucine'. The results indicated that as the number of $-CH_2$ groups in the alkyl chain of potassium alkanoates, i.e. surfactant alkyl chain length gets longer (shorter), the formation of the Ch_D phase (Ch_B and/or Ch_C phase) is more favored. In other words, the surfactant alkyl chain length plays an important role on the formation of different cholesteric phases and on the cholesteric uniaxial to cholesteric biaxial phase transitions.

3. MATERIALS AND METHOD

3.1 Materials

All chemicals (undecanoic acid, dodecanoic acid, tridecanoic acid, absolute ethanol, toluene, diethylether, potassium hydroxide), except surfactants, were purchased from Sigma, Merck, Alfa-Aesar with purities of >99%. A water-based ferrofluid was commercially available from Ferrotec (EMG-605). Ultrapure water was provided by Millipore Direct-Q3 UV (18,2 M Ω ·cm of resistivity at 25 °C) for the preparation of lyotropic liquid crystal samples.

A rotatory evaporator (Heidolph HeiVap), electronic balance (Radwag AS220, five digits), vortex (IKA 4 basic), centrifuge (Hettich Zentrifugen EBA 20), magnetic stirrer (Heidolph MR Hei-End), an ultrasonic cleaner (Isolab), a photopolymerizer (3M Elipar), a gaussmeter (Lakeshore 475 DSP), a polarizing optical microscope (Nikon Eclipse E200POL) with a NIS-Element software and a Nikon camera, microsyringes (Hamilton, 5 and 10 μ L), a vacuum oven (Nüve EV018) and a vacuum pump (Vacuubrand RZ2.5) were used.

Surfactant molecules (potassium undecanoate, KC11; potassium dodecanoate, KC12; potassium tridecanoate, KC13) were synthesized from the neutralization of the undecanoic acid, dodecanoic acid and tridecanoic acid, respectively, with ethanolic KOH according to the well-described procedure given in the literature (Berejnov, et. al., 2000). The neutralization reaction was carried out at room temperature (~24-25°C) by controlling the pH of the reaction mixture and completed in 2h. While the reaction was proceeding the pH was kept at 10.80 by adding the 10% ethanolic KOH. The removal of non-neutralized acids from the products of KC11, KC12, and KC13 is an important key point to obtain reproducible and reliable results. To do so, before recrystallization of the potassium alkanoates, they added in the hot toluene and filtered off under vacuum. All three potassium alkanoates were characterized by FT-IR (Figures 3.2-3.4) after they were recrystallized from ethanol

at least three times. The disappearances of bands related to carboxyl group, $-\text{COOH}$ at $\sim 1700\text{ cm}^{-1}$, and hydroxyl group, $-\text{OH}$ at $850\text{--}960\text{ cm}^{-1}$, $1240\text{--}1300\text{ cm}^{-1}$ and $2500\text{--}3400\text{ cm}^{-1}$, and the appearance of potassium carboxylate, $-\text{COO}^-\text{K}^+$, band at $\sim 1550\text{ cm}^{-1}$ confirmed that undecanoic acid, dodecanoic acid and tridecanoic acid were completely neutralized into KC11, KC12, and KC13, respectively.

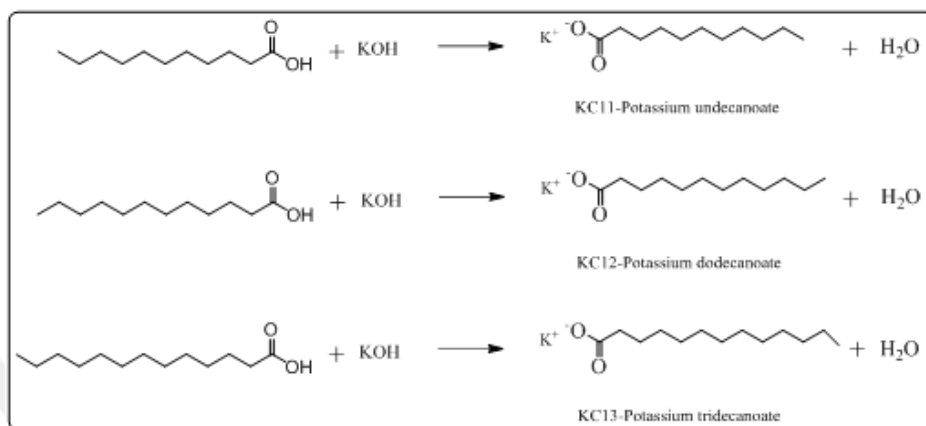


Figure 3.1. Scheme of the synthesis of surfactants KC11, KC12 and KC13.

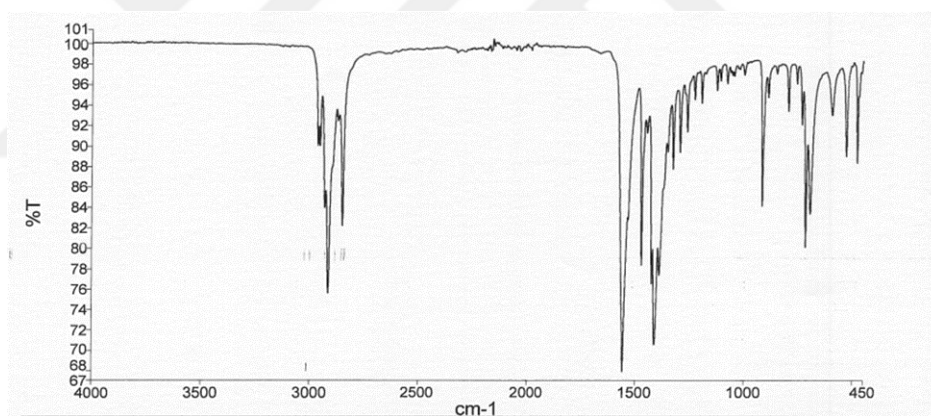


Figure 3.2. FT-IR spectrum of KC11.

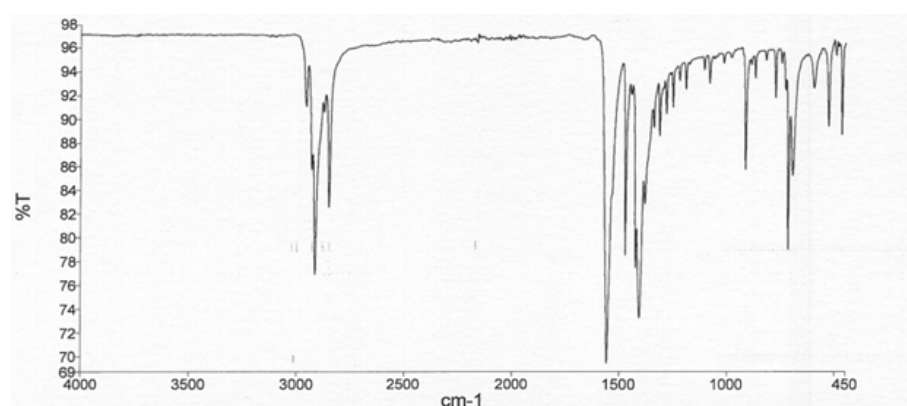


Figure 3.3. FT-IR spectrum of KC12.

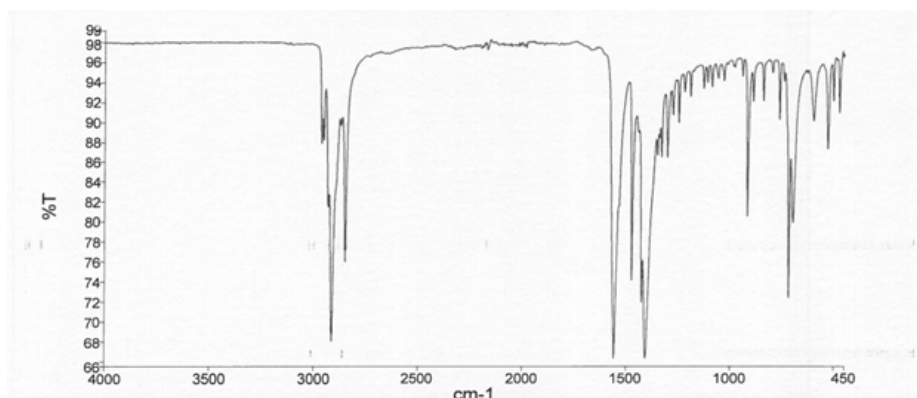


Figure 3.4. FT-IR spectrum of KC13.

3.2 Preparation of Lyotropic Liquid Crystal Samples

Lyotropic liquid crystal samples were prepared by weighing appropriate amounts of the ingredients (potassium alkanoates, potassium sulfate, decanol, water and brucine) into the pyrex test tubes which were closed by their caps and then parafilm to prevent water loss. Homogeneous samples were obtained in three steps: (a) leaving the test tubes in a water bath of $\sim 50\text{-}60\text{ }^{\circ}\text{C}$ for 5 min, (b) applying vortex with 3000 rpm for 5 min, and (c) centrifuging with 4500 rpm for 5 min. These three steps were applied occasionally until well-homogenized samples were obtained. If some part of undissolved potassium sulfate was seen at the bottom of the test tube, the ultrasonic cleaner was additionally used to provide faster dissolving of potassium sulfate. For the formation of well-aligned cholesteric stripes in relatively short times, a water-based ferrofluid was added to the samples as $1\text{ }\mu\text{L}$ ferrofluid per 2.5 g of the sample. The experimental studies indicated that this amount of ferrofluid doping does not modify the phase topology and the uniaxial-to-biaxial phase transitions (L. Li'ebert and A. M. Figueiredo Neto, 1984).

3.3 Polarizing Optical Microscopy Measurements

The ferrofluid-doped samples were transferred into the microslides of 0.2 mm thickness, whose ends were closed well with a specific photopolymer to prevent the water loss. The microslides were put in a heating/freezing stage (Linkam LTS120E), connected to a temperature controller (Linkam T95-PE). The temperature stability

was provided by a water circulating bath (Polyscience SD07R). A magnetic field of ~ 0.9 kG was applied to obtain well-aligned cholesteric phases. Then, the textures of the cholesteric phases were characterized, and the cholesteric uniaxial-to-cholesteric biaxial phase transitions were determined using the polarising optical microscopy measurements.



4. RESULT AND DISCUSSION

Table 1 and 2 show the compositions of KC11/KC12 and KC12/KC13 lyotropic mixtures, respectively. The starting mixture s1, KC12/K₂SO₄/DeOH/water/brucine, was chosen from the literature (D Reis, et al., 2013). The uniaxial-to-biaxial phase transitions of the sample s1 are in a good agreement with those given in the (D Reis, et al., 2013) within the experimental error. As seen from the tables, for both KC11/KC12 and KC12/KC13, some part of KC12 was replaced with KC11 and KC13, separately, by keeping the total surfactant concentration (in mole percent) constant.

Table 4.1. Lyotropic mixture compositions in mole % for KC11/KC12 binary system.

Sample	KC11	KC12	K ₂ SO ₄	DeOH	H ₂ O	Brucine
s1	0.00	3.82	0.60	1.14	94.34	0.10
s2	0.38	3.44	0.60	1.14	94.34	0.10
s3	0.76	3.06	0.60	1.14	94.33	0.10
s4	1.15	2.68	0.60	1.14	94.34	0.10
s5	1.53	2.29	0.60	1.14	94.34	0.10

Table 4.2. Lyotropic mixture compositions in mole % for KC12/KC13 binary system.

Sample	KC13	KC12	K ₂ SO ₄	DeOH	H ₂ O	Brucine
s1	0.00	3.82	0.60	1.14	94.34	0.10
s6	0.38	3.44	0.60	1.14	94.34	0.10
s7	0.76	3.06	0.60	1.14	94.33	0.10
s8	1.15	2.68	0.60	1.14	94.34	0.10
s9	1.53	2.29	0.60	1.14	94.34	0.10

The lyotropic cholesteric samples were characterized by the polarizing optical microscope as a function of temperature, i.e. the textural analyses were carried out and the uniaxial-to-biaxial phase transitions were determined. The uniaxial-to-biaxial phase transitions were performed starting from the Ch_D phase. To do so, first the sample was well-aligned in the presence of the magnetic field for some hours at a fixed temperature. Then, by changing temperature, the phase transition temperatures were evaluated. In the Figure 4.1-4.9, the cholesteric textures of the samples s1-s9 were given in details.



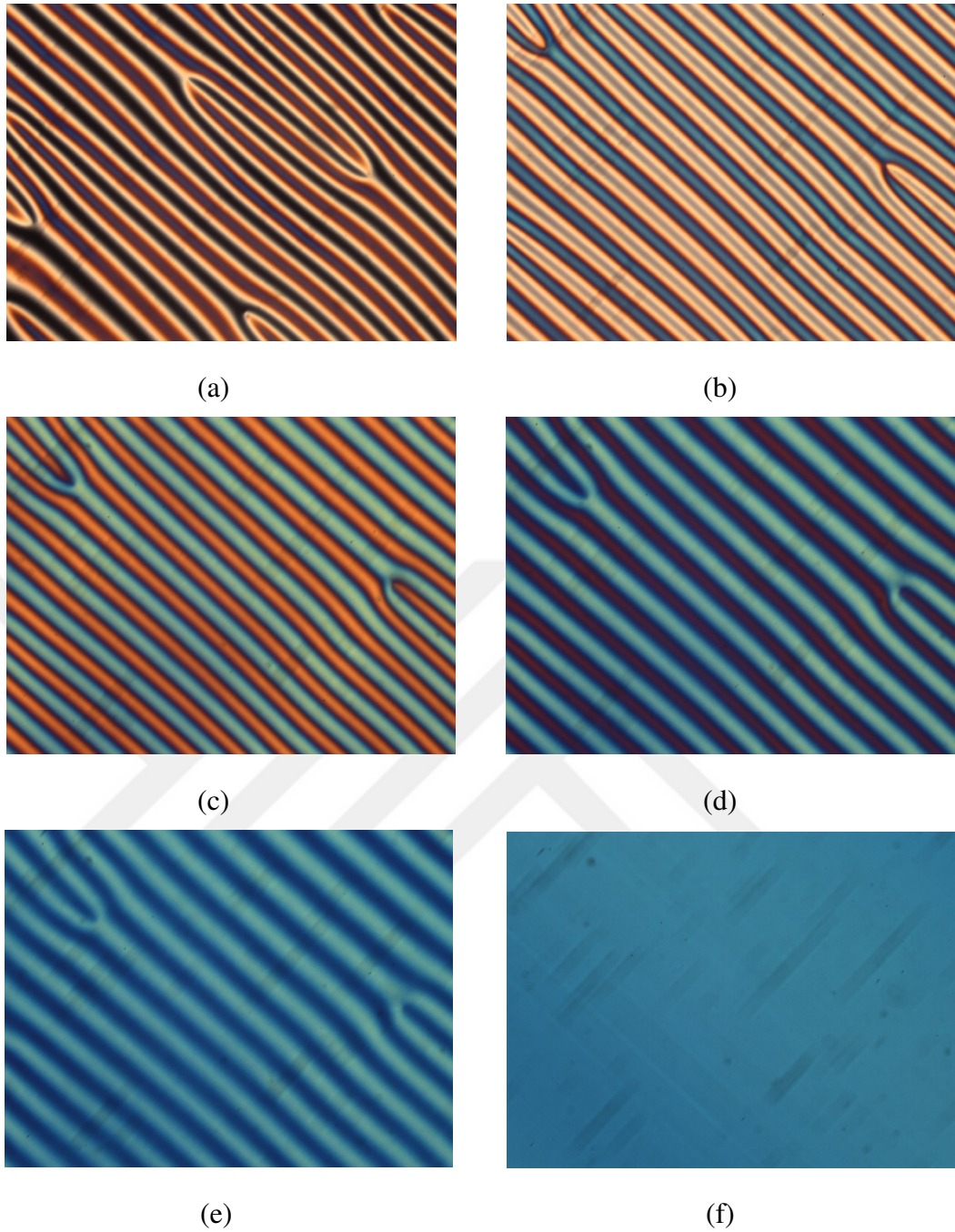


Figure 4.1. POM textures of the sample s1: (a) 30.00°C, Ch_D; (b) 21.60°C, Ch_B; (c) 18.50°C, Ch_B; (d) 16.50°C, Ch_B; (e) 15.00°C, Ch_B; (f) 14.00°C, Ch_C. The sample was aligned in the magnetic field during 16 h to obtain well-aligned Ch_D phase. The sample thickness is 0.2 mm, and the magnification of the objective is 10x.

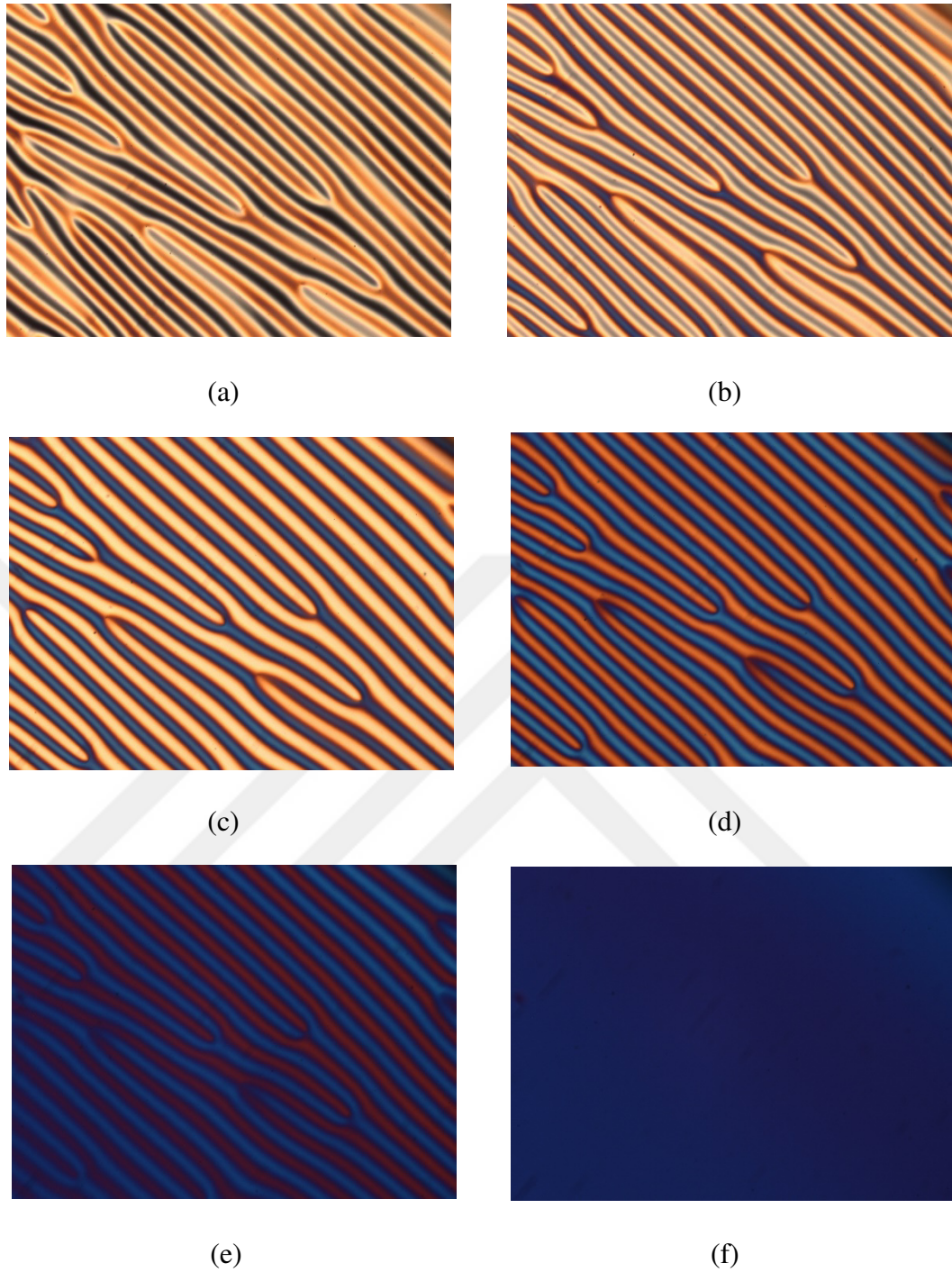


Figure 4.2. POM textures of the sample s2: (a) 30.00°C, Ch_D; (b) 22.50°C, Ch_B; (c) 21.50°C, Ch_B; (d) 19.50°C, Ch_B; (e) 18.50°C, Ch_B; (f) 18.00°C, Ch_C. The sample was aligned in the magnetic field during 12 h to obtain well-aligned Ch_D phase. The sample thickness is 0.2 mm, and the magnification of the objective is 10x.

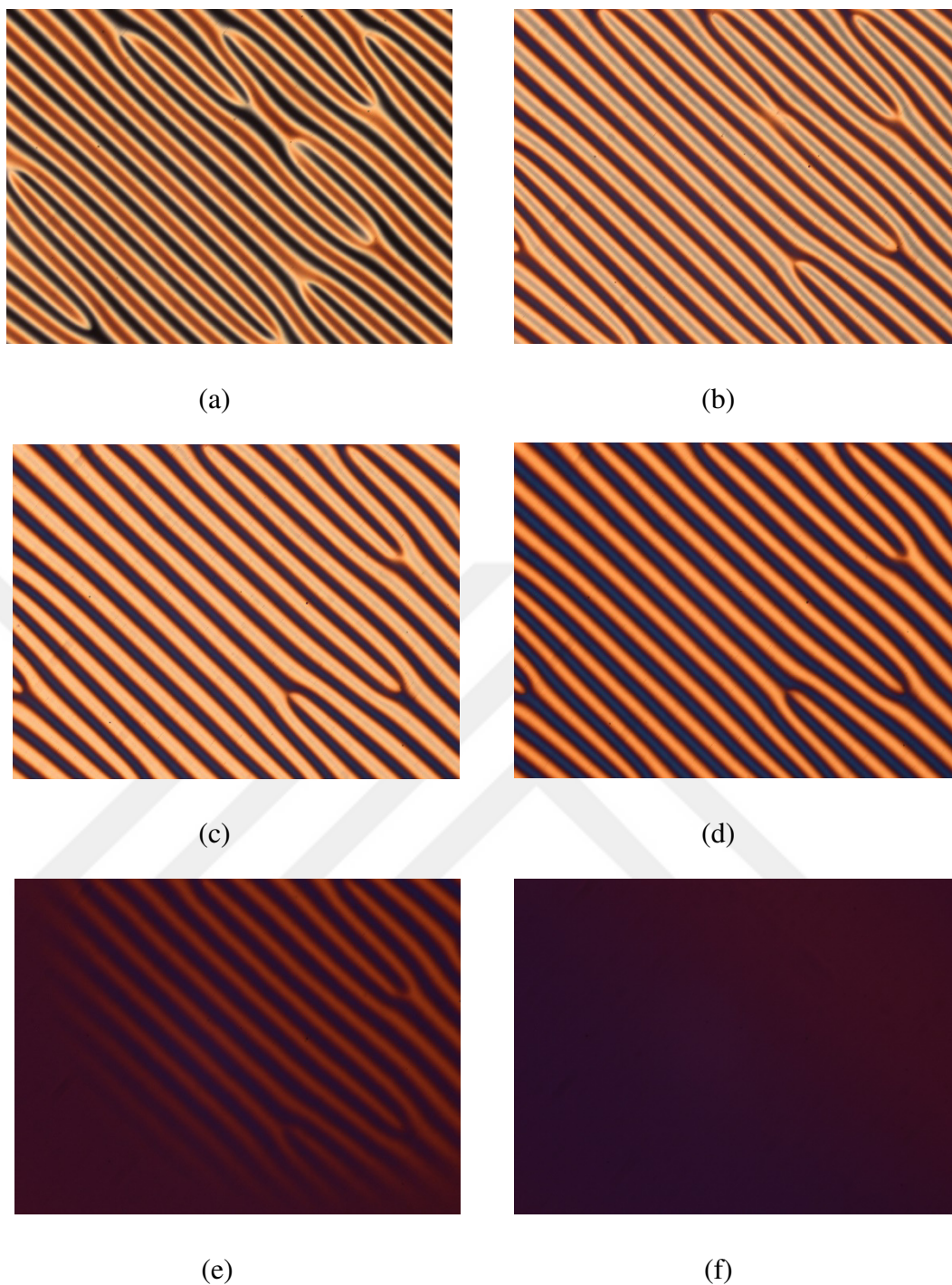


Figure 4.3. POM textures of the sample s3: (a) 30.00°C, Ch_D ; (b) 24.10°C, Ch_B ; (c) 23.71°C, Ch_B ; (d) 22.66°C, Ch_B ; (e) 21.66°C, Ch_B (at the Ch_B - Ch_C transition); (f) 21.16°C, Ch_C . The sample was aligned in the magnetic field during 13 h to obtain well-aligned Ch_D phase. The sample thickness is 0.2 mm, and the magnification of the objective is 10x.

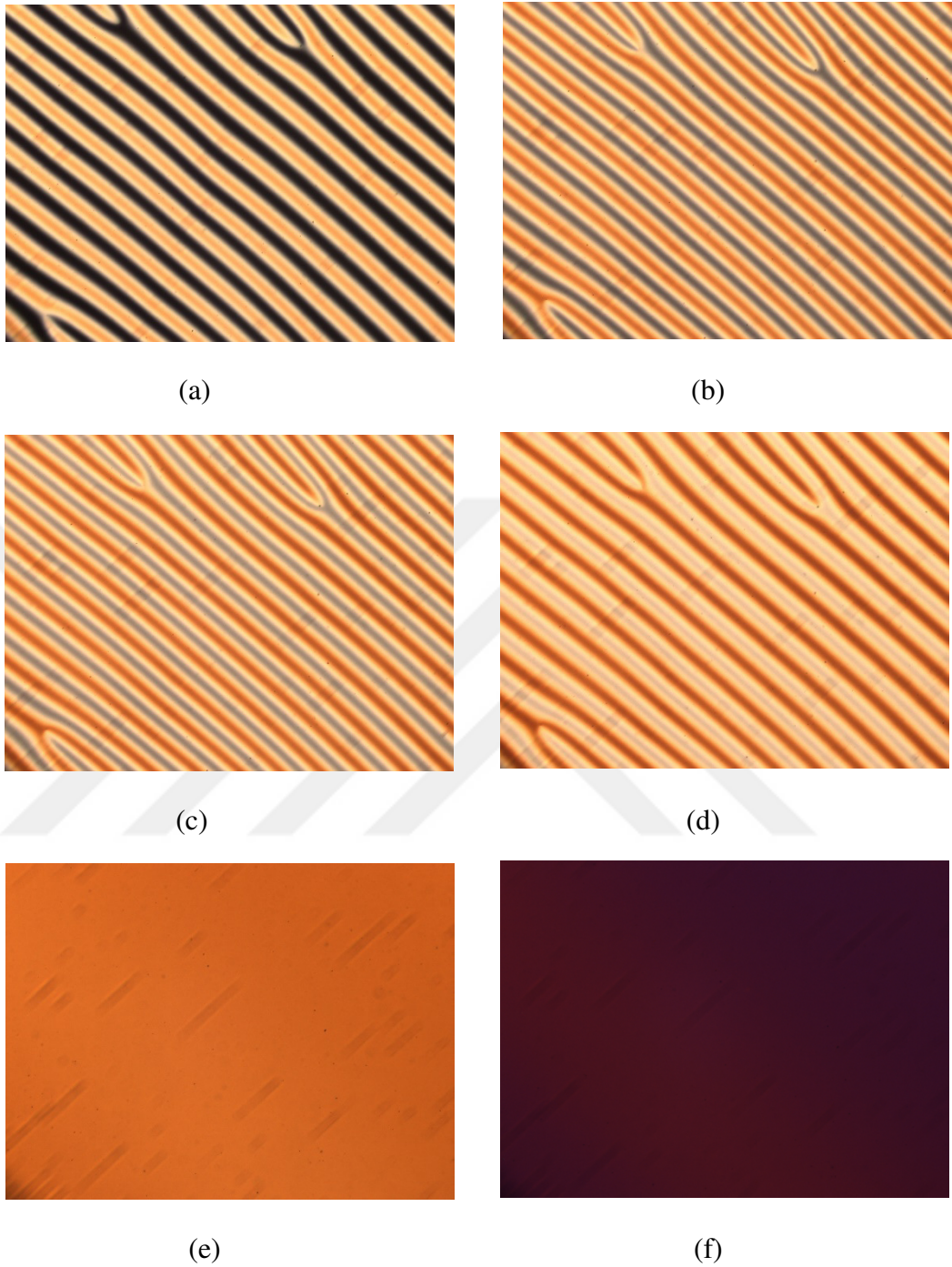


Figure 4.4. POM textures of the sample s4: (a) 30.00°C, Ch_D; (b) 25.99°C, Ch_B; (c) 25.87°C, Ch_B; (d) 25.62°C, Ch_B; (e) 24.50°C, Ch_C; (f) 20.00°C, Ch_C. The sample was aligned in the magnetic field during 12 h to obtain well-aligned Ch_D phase. The sample thickness is 0.2 mm, and the magnification of the objective is 10x.

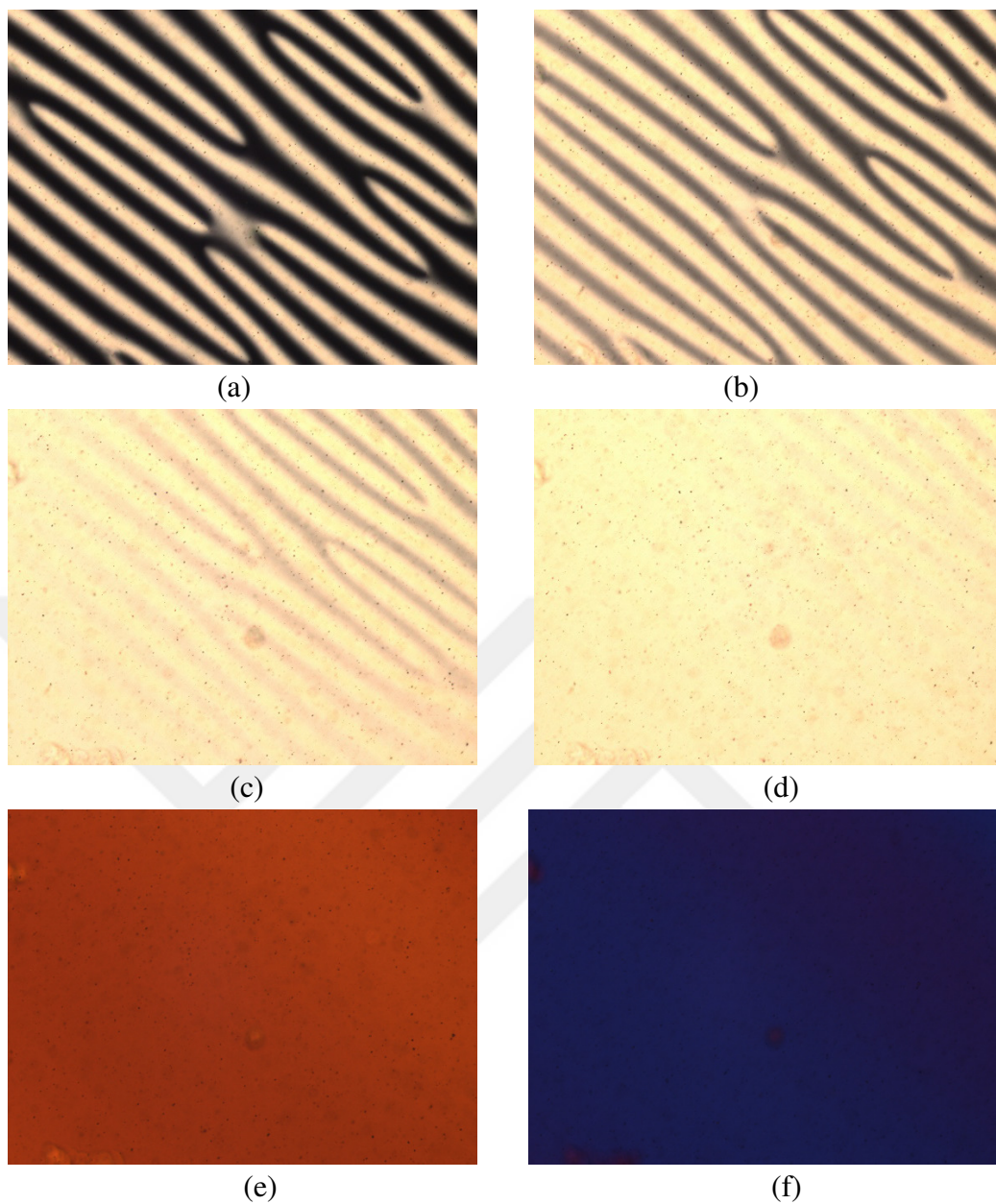


Figure 4.5. POM textures of the sample s5: (a) 30.00°C, Ch_D; (b) 28.04°C, Ch_B (near the Ch_D-Ch_B transition); (c) 27.84°C, Ch_B (at the Ch_B-Ch_C); (d) 27.74°C, Ch_C; (e) 20.00°C, Ch_C; (f) 10.00°C, Ch_C. The sample was aligned in the magnetic field during 12 h to obtain well-aligned Ch_D phase. The sample thickness is 0.2 mm, and the magnification of the objective is 10x.

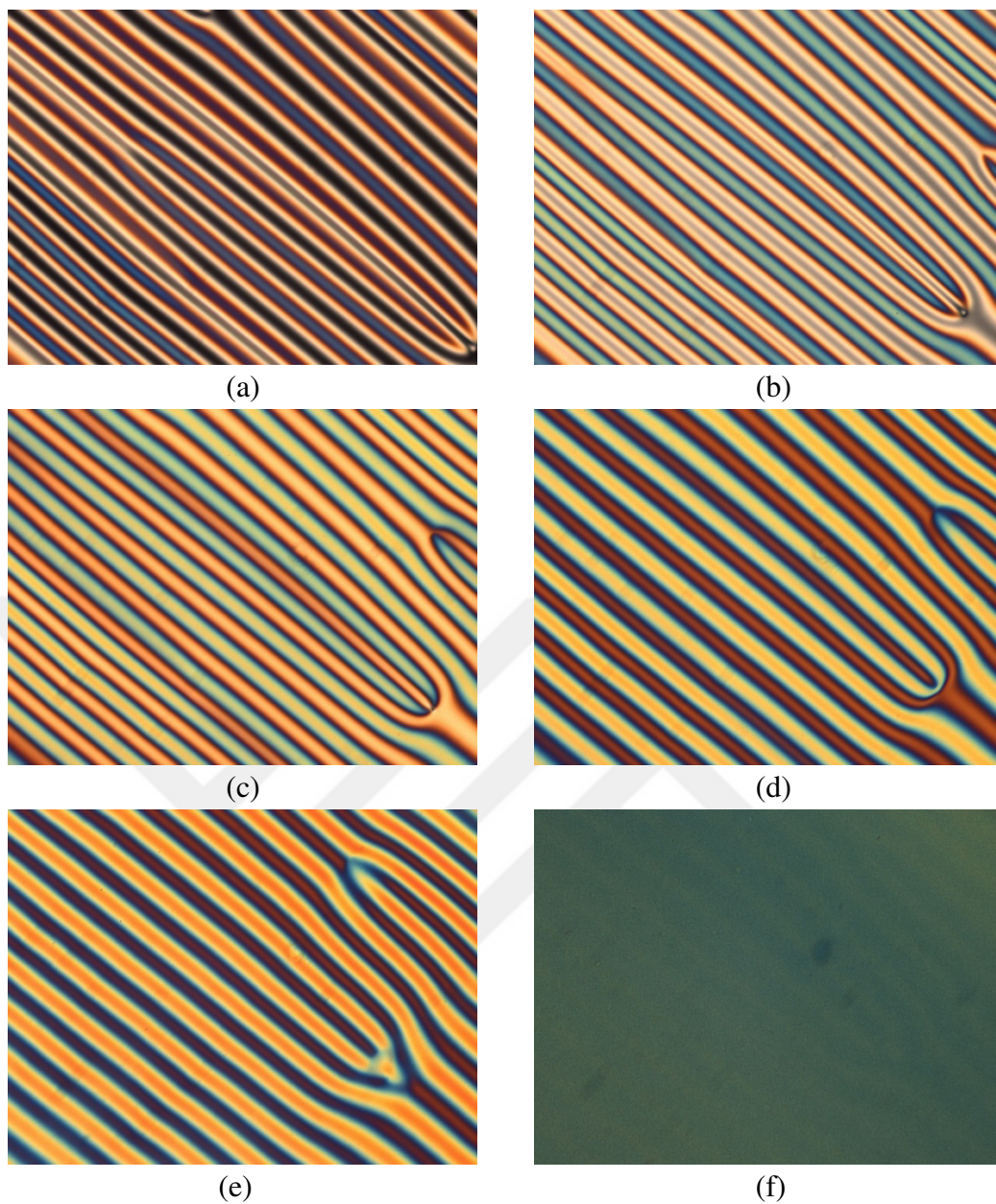


Figure 4.6. POM textures of the sample s6: (a) 30.00°C, Ch_D ; (b) 19.99°C, Ch_B (near the Ch_D - Ch_B transition); (c) 18.00°C, Ch_B ; (d) 15.00°C, Ch_B ; (e) 08.00°C, Ch_B (near the Ch_B - Ch_C transition); (f) 07.50°C, Ch_C . The sample was aligned in the magnetic field during 10 h to obtain well-aligned Ch_D phase. The sample thickness is 0.2 mm, and the magnification of the objective is 10x.

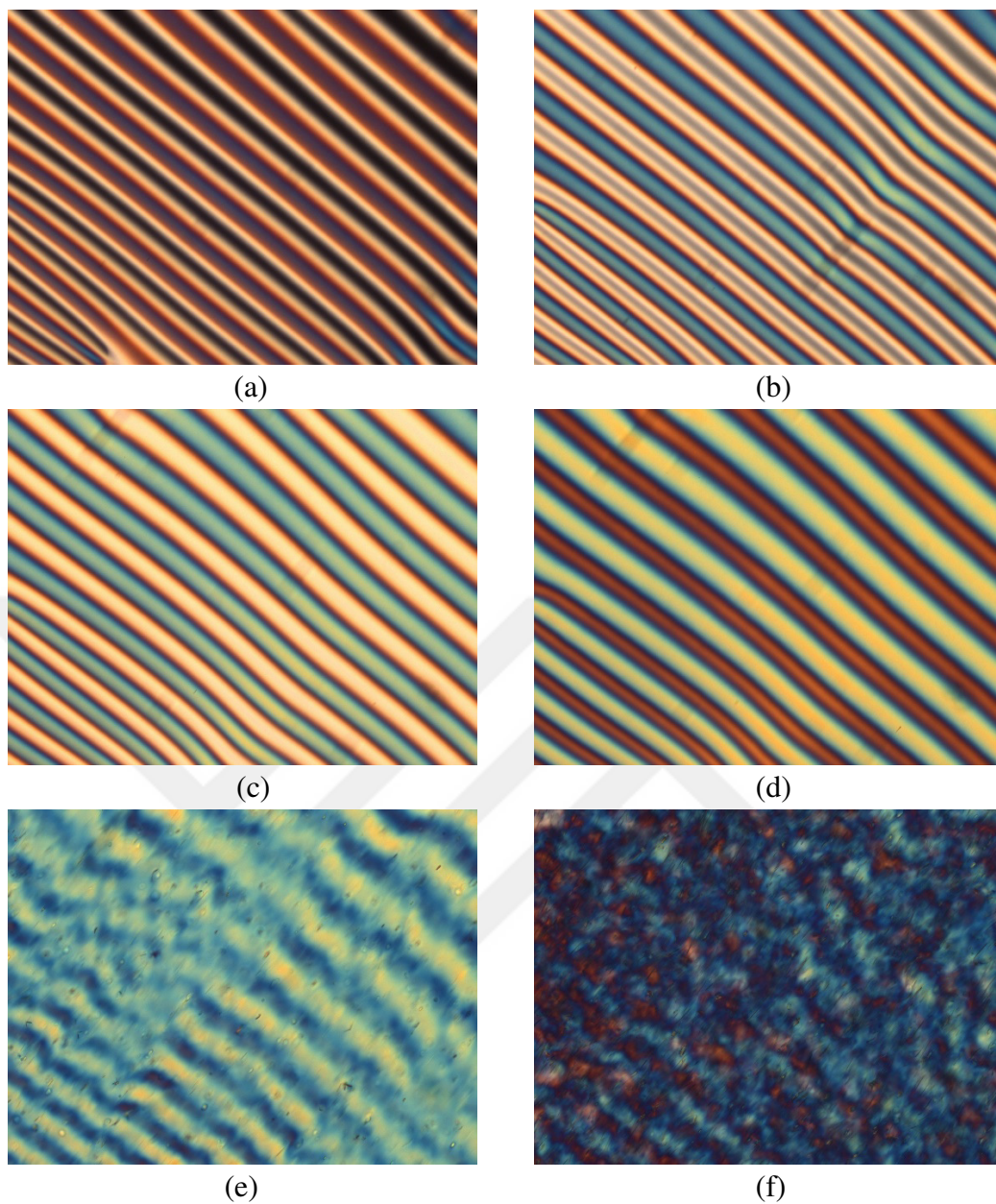


Figure 4.7. POM textures of the sample s7: (a) 30.00°C, Ch_D ; (b) 19.01°C, Ch_B (near the Ch_D - Ch_B transition); (c) 18.00°C, Ch_B ; (d) 13.50°C, Ch_B ; (e) 06.00°C, two-phase region; (f) 05.50°C, crystalline- or gel-like phase. The sample was aligned in the magnetic field during 10 h to obtain well-aligned Ch_D phase. The sample thickness is 0.2 mm, and the magnification of the objective is 10x.

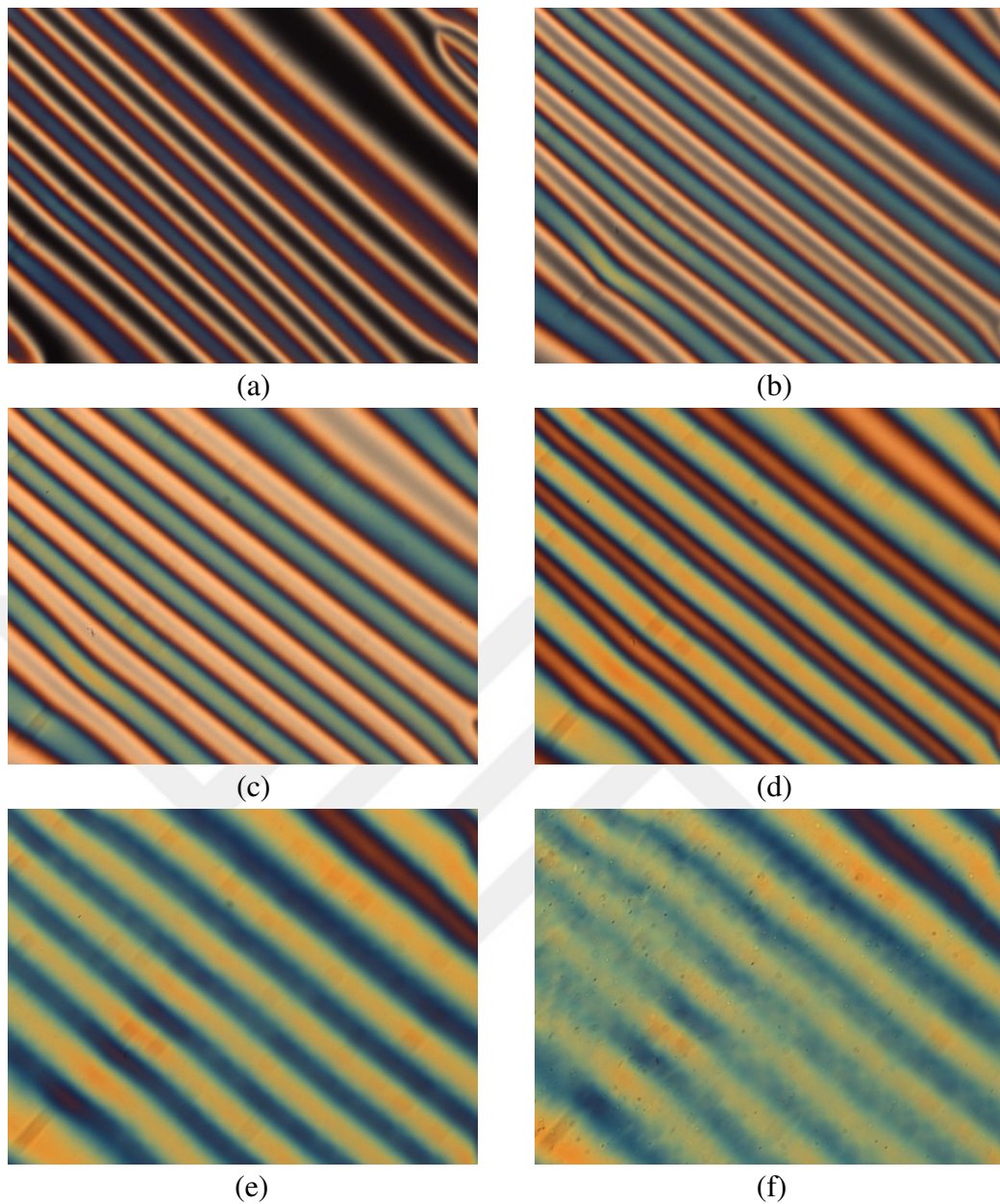


Figure 4.8. POM textures of the sample s8: (a) 30.00°C, Ch_D ; (b) 18.10°C, Ch_B (near the Ch_D - Ch_B transition); (c) 17.20°C, Ch_B ; (d) 12.70°C, Ch_B ; (e) 07.20°C, Ch_B (near the Ch_B -two-phase transition); (f) 05.00°C, two-phase region;. The sample was aligned in the magnetic field during 12 h to obtain well-aligned Ch_D phase. The sample thickness is 0.2 mm, and the magnification of the objective is 10x.

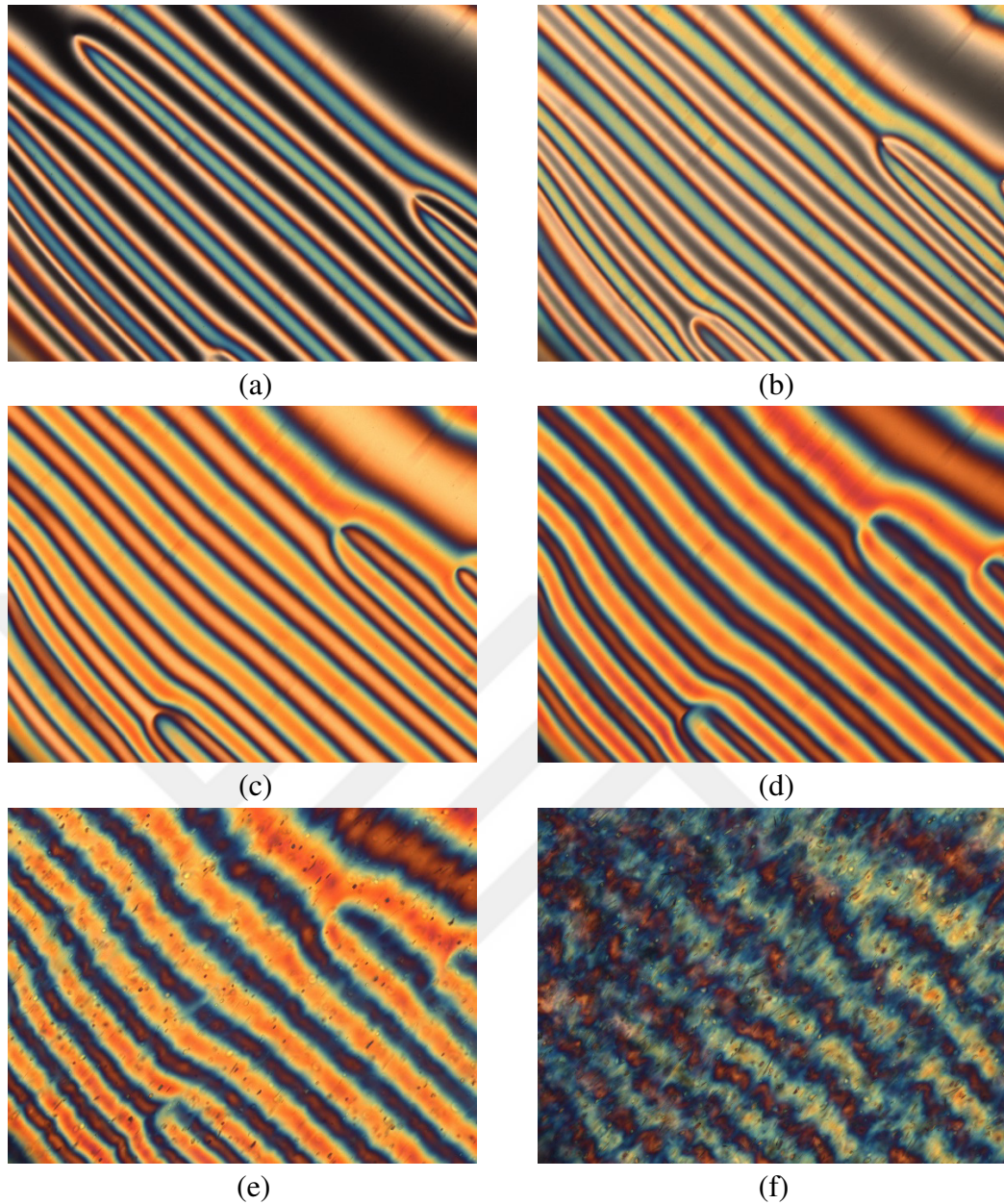


Figure 4.9. POM textures of the sample s9: (a) 30.00°C, Ch_D ; (b) 16.94°C, Ch_B (near the Ch_D - Ch_B transition); (c) 13.50°C, Ch_B ; (d) 09.00°C, Ch_B ; (e) 06.00°C, Ch_B (near the Ch_B -two-phase transition); (f) 05.50°C, two-phase region; the sample was aligned in the magnetic field during 13 h to obtain well-aligned Ch_D phase. The sample thickness is 0.2 mm, and the magnification of the objective is 10x.

The phase transitions from uniaxial cholesterics to biaxial cholesteric are of subject to this thesis, but others not. So, we give the uniaxial to biaxial phase transitions in the Table 4.3 and 4.4. As seen from these tables and the polarizing optical microscopy textures, while we observed the Ch_B - Ch_C phase transition for the

KC11/KC12 mixtures, however, we could obtain only one sample (s6), which exhibits Ch_B - Ch_C phase transition in addition to the Ch_D - Ch_B one, for the KC12/KC13. The reason may be attributed to the formation of the gel-like phase at lower temperatures before the Ch_B - Ch_C phase transition.

Table 4.3. The cholesteric to cholesteric phase transitions for KC11/KC12 binary system.

Sample	Phase Transitions		
s1	Ch_D	$\xrightarrow{21.90^\circ C}$	$Ch_B \xrightarrow{14.42^\circ C} Ch_C$
s2	Ch_D	$\xrightarrow{22.64^\circ C}$	$Ch_B \xrightarrow{18.32^\circ C} Ch_C$
s3	Ch_D	$\xrightarrow{24.34^\circ C}$	$Ch_B \xrightarrow{21.66^\circ C} Ch_C$
s4	Ch_D	$\xrightarrow{26.08^\circ C}$	$Ch_B \xrightarrow{25.31^\circ C} Ch_C$
s5	Ch_D	$\xrightarrow{28.12^\circ C}$	$Ch_B \xrightarrow{27.84^\circ C} Ch_C$

Table 4.4. The cholesteric to cholesteric phase transitions for KC12/KC13 binary system.

Sample	Phase Transitions		
s1	Ch_D	$\xrightarrow{21.90^\circ C}$	$Ch_B \xrightarrow{14.42^\circ C} Ch_C$
s6	Ch_D	$\xrightarrow{20.35^\circ C}$	$Ch_B \xrightarrow{07.80^\circ C} Ch_C$
s7	Ch_D	$\xrightarrow{19.17^\circ C}$	$Ch_B \xrightarrow{no} Ch_C$
s8	Ch_D	$\xrightarrow{18.34^\circ C}$	$Ch_B \xrightarrow{no} Ch_C$
s9	Ch_D	$\xrightarrow{17.08^\circ C}$	$Ch_B \xrightarrow{no} Ch_C$

The transition temperatures were used to construct the partial phase diagrams of both systems in the Figure 4.10 and 4.11, considering the uniaxial to biaxial cholesteric phase transitions given in the Tables 4.3 and 4.4, respectively.

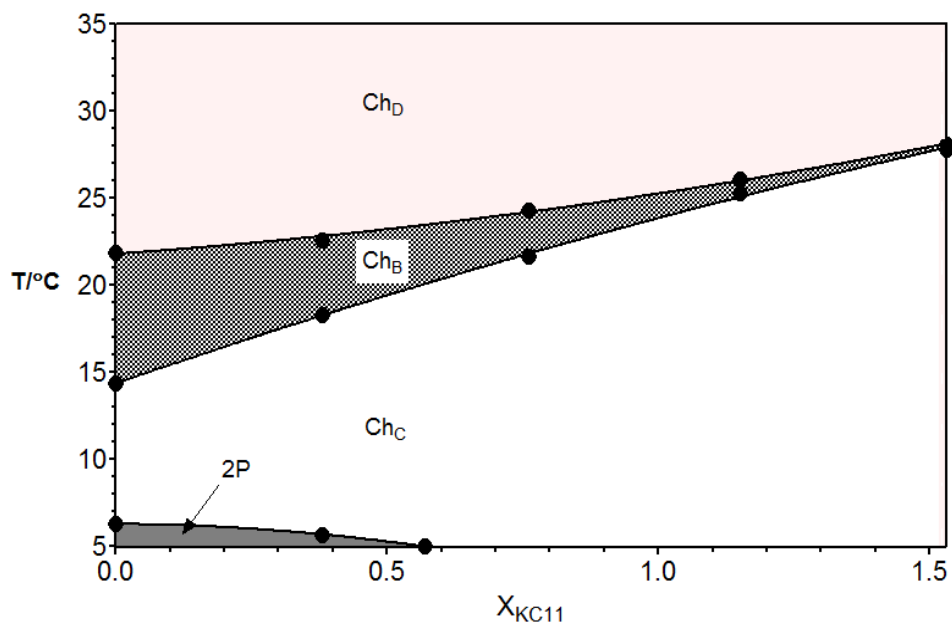


Figure 4.10. The partial phase diagram of the KC11/KC12 binary surfactant system as a function of the increase in the KC11 concentration in the mixtures. 2P: two-phase region.

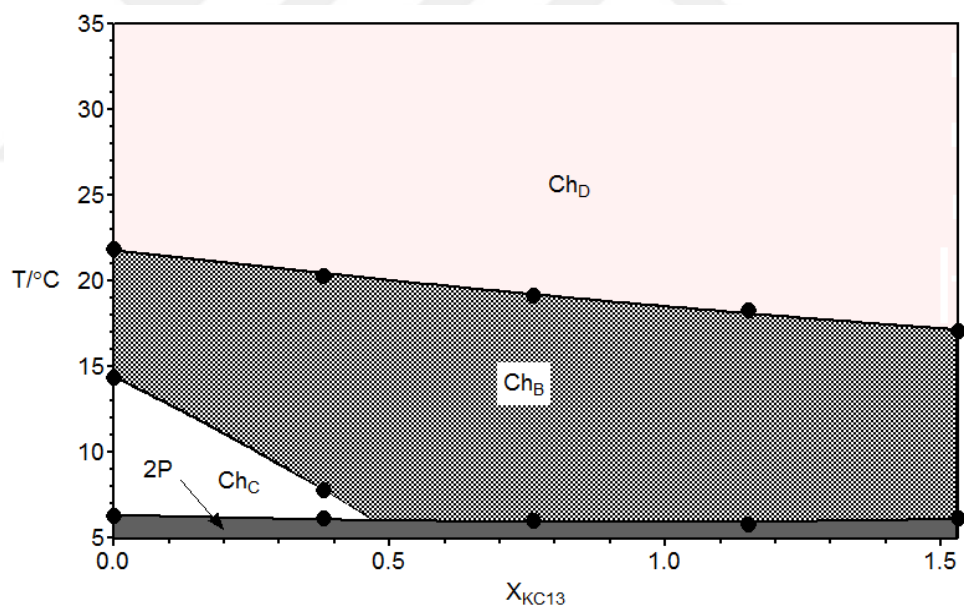


Figure 4.11. The partial phase diagram of the KC12/KC13 binary surfactant system as a function of the increase in the KC13 concentration in the mixtures. 2P: two-phase region.

As seen in the Figure 4.10, when the concentration of the KC11 is increased in the binary KC11/KC12 mixtures at the constant total surfactant concentration, i.e. the total number of the surfactants is constant in all the mixtures, the Ch_D and the Ch_B phase regions diminish and the Ch_C phase region gets larger. In the case of the KC12/KC13 mixtures, the increase in the concentration of KC13 gives rise to the

increase in the Ch_D and the Ch_B regions but to the decrease in the Ch_C region, Figure 4.11. In the Figure 4.12, the results of the both systems are used to construct the complete phase diagram to show the effect of the surfactant alkyl chain length on the cholesteric phase regions and the uniaxial-to-biaxial phase transitions. The Figure 4.12 clearly shows that the surfactant alkyl chain length affects the formation of different lyotropic cholesteric phases and the uniaxial to biaxial cholesteric phase transitions. As the surfactant alkyl chain length gets longer (shorter), it is most likely to be obtained the Ch_D (Ch_C) phase. At the intermediate level of the surfactant alkyl chain length, it is possible to obtain the lyotropic Ch_B phase and the Ch_B region is highly dependent of the surfactant alkyl chain length, Figure 4.13. From the phase transition temperatures point of view, the increase in the surfactant alkyl chain length causes shifting the Ch_D - Ch_B and Ch_B - Ch_C phase transitions towards the lower temperatures.

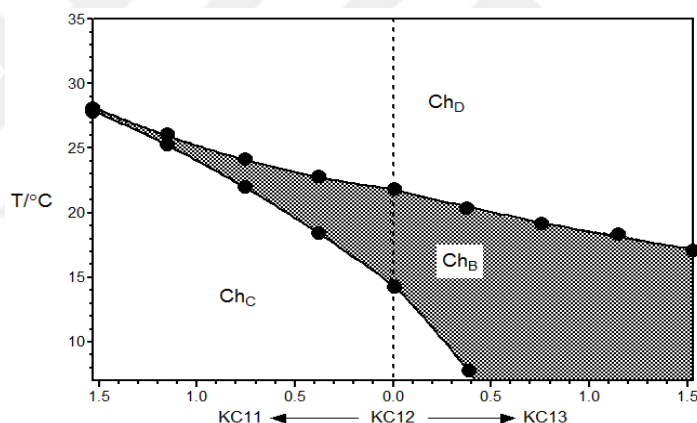


Figure 4.12. Combining the phase transition temperatures of the KC11/KC12 mixtures with those of the KC12/KC13 mixtures. The zero point, which is shown by a vertical dashed-line, corresponds to the sample s1, i.e. a single surfactant system (KC12). To the left from the zero point, the concentration of the KC11 (X_{KC11}) increases in the mixtures of the KC11/KC12. By the same way, to the right from the zero point, the concentration of the KC13 (X_{KC13}) increases in the mixtures of the KC12/KC13. In this partial phase diagram, the 2P-regions observed in the Figure 4.10 and 4.11 were ignored by starting the y-axis from 7.00°C.

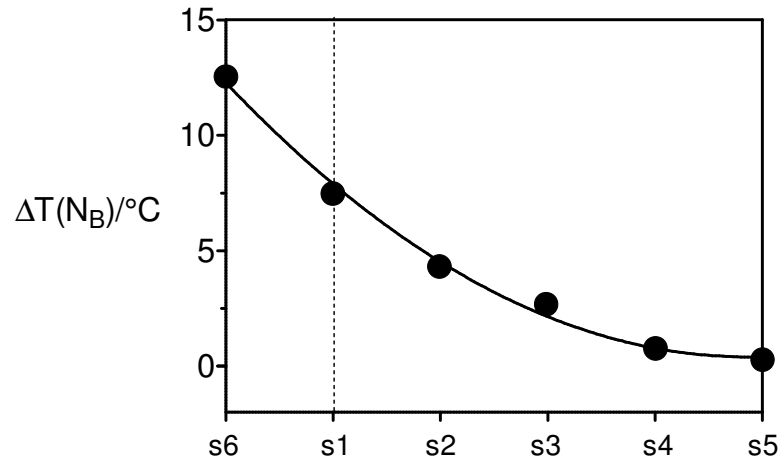


Figure 4.13. Combining the biaxial phase region of the KC11/KC12 mixtures with those of the KC12/ KC13 mixtures. The vertical dashed line corresponds to a single surfactant system (KC12). While the concentration of the KC11 increases in the mixtures of the KC11/KC12 from s1 to s5, the concentration of the KC13 increases in the mixtures of the KC12/ KC13 from s1 to s6.

Summarily, if the results shown in the Figure 4.12 and 4.13 are considered, the surfactant alkyl chain length seems as an important parameter to obtain different lyotropic cholesteric phases, especially the biaxial one. Similar results were obtained from the lyotropic nematic mixtures of some potassium alkanooates and sodium alkylsulfates in the (Cihan, 2018). In that study, the authors investigated the effect of the surfactant alkyl chain length on the stabilization of different lyotropic nematic phases from laser conoscopy, polarizing optical microscopy and small-angle X-ray scattering. Their results indicated that the increase (decrease) in the number of $-\text{CH}_2$ groups of the surfactant molecule, the lyotropic discotic nematic phase, N_D (calamitic nematic phase, N_C), is stabilized. Similar to our results, the N_B is stabilized for the intermediate level of the number of $-\text{CH}_2$ groups. Indeed, the formation of different nematic phases arises from the change in the “micellar shape anisotropy”. It means that when the increase in the surfactant alkyl chain length gives rise to the increase in the micellar shape anisotropy for both lyotropic nematic and cholesteric phases. From this respect, it may be concluded that the micellar shape anisotropy controls the stabilizing different lyotropic cholesteric phases.

5. CONCLUSIONS

In the frame of this thesis, we studied the effect of the surfactant alkyl chain length on the formation or stabilization of different lyotropic cholesteric phases. The results indicated that the surfactant alkyl chain length plays an important role on the formation of lyotropic Ch_D , Ch_B and Ch_C phases. Because the surfactant alkyl chain length is correlated with the micellar shape anisotropy as proved by small-angle X-ray scattering experiments (Neto and Salinas, 2005), i.e. the longer the surfactant alkyl chain the higher the micellar shape anisotropy, the Ch_D and/or Ch_B phase domains in the partial phase diagrams get larger as the micellar shape anisotropy increases. By the same way, if the micelles have smaller shape anisotropy it is highly possible that the Ch_C phase is observed.

Furthermore, the increase in the micellar shape anisotropy affects the uniaxial-to-biaxial phase transition temperatures. As the micellar shape anisotropy, or the surfactant alkyl chain length, increases the uniaxial-to-biaxial phase transitions (Ch_D - Ch_B and Ch_B - Ch_C) shift to the lower temperatures.

From these respects, this study shows, to the best of our knowledge, for the first time the effect of the surfactant alkyl chain length on the stabilization of different lyotropic cholesteric phases.

6. REFERENCES

- Acimis, M. and Reeves, L.W., (1980), "A Type-II Aqueous Cholesteric Lyomesophase", *Can. J. Chem.*, 58, 1533-1541.
- Akpinar E, Acimis M, Ocak Ç (2001) "Strange mass density behaviour of a micellar chiral nematic phase composed of an amphiphilic racemic mixture and its Lenantiomer", *Physical Chemistry Chemical Physics*, 3:645-646.
- Akpinar E , Otluoğlu K, Turkmen M, Canioz C, Reis D, Neto AMF (2016) "Effect of the presence of strong and weak electrolytes on the existence of uniaxial and biaxial nematic phases in lyotropic mixtures", *Liquid Crystals*, 43(16): 1693 - 1708.
- Akpinar E, Turkmen M, Canioz C, Neto AMF (2016) "Role of kosmotrope chaotrope interactions at micelle surfaces on the stabilization of lyotropic nematic phases", *European Physical Journal E*, 39(11), 107(1-16).
- Akpinar E, Cihan Canioz, Meric Turkmen, Dennys Reis & Antônio Martins Figueiredo Neto (2017) "Effect of the surfactant alkyl chain length on the stabilisation of lyotropic nematic phases," *Liquid Crystals*.
- Alcantara MR and Vanin JA, (1984), Optical Sign Determinations on Cholesteric Lyotropic Mesophases, *Mol. Cryst. Liq. Cryst.*, 107, 333- 340.
- Antonio M Figueiredo Neto And Silvio R. A. Salinas 'The Physics Of Lyotropic Liquid Crystals Phase Transitions And Structural Properties' First Edition, Oxford University Press 2005
- Badikov V, Mitin K, Noack F, Panyutin V, Petrov V, Seryogin A and Shevyrdyaeva G (2009), 'Orthorhombic nonlinear crystals of Ag_xGaxGe_{1-x}Se₂ for the mid-infrared spectral range', *Opt. Mater.* 31, 590–597
- Berejnov V V, Cabuil V, Perzynski R, Raikher YL, Lysenko SN, & Sdobnov V N J CR (2000). Lyotropic nematogenic system potassium laurate-1-decanol-water: Method of synthesis and study of phase diagrams. 45(3), 493-500.
- Braga WS, Santos OR, Luders DD, (2013) Conoscopic image of a biaxial negative nematic phase in a potassium laurate-decanol-D₂O mixture. *J Mol Liq.*; 187:20–23.
- Brand HR, Pleiner H. (1989) "Cholesteric to cholesteric phase transitions in liquid crystals", *J Phys Lett*, 46:711–718.

- Carnero Ruiz C, (1999), "Thermodynamics of micellization of tetradecyltrimethylammonium bromide in ethylene glycol-water binary mixtures" *Colloid Polym Sci* 277:701-707
- Chattopadhyay A and Erwin L (1984) "Fluorimetric determination of critical micelle concentration avoiding interference from detergent charge", *Analytical Biochemistry*, 139(2):408-412.
- Boden N, Jackson PH, McMullen K and Holmes MC, (1979), Are "nematic" amphiphilic liquid crystalline mesophases thermodynamically stable? *Chem. Phys. Lett.*, 65, 476-479.
- Boden N, Radley K, Holmes MC (1981) "On the relationship between the micellar structure and the diamagnetic anisotropy of amphiphilic nematic mesophases", *Molecular Physics*, 42, 493-496.
- De Jeu, WH, (1980), *Physical Properties of Liquid Crystalline Materials*, Gordon and Breach Science Publishers Ltd., Ch. 4, pp.34.
- De Sant'Ana, ZA; Neto, AMF, (1992) Uniaxial-to-biaxial cholesteric and nematic phase transitions on a lyotropic alcohol-free mixture. *Phys. Rev. A*, 46, 7630-7635).
- Debye P," Die van der Waalsschen Kohasion-skrafte" *Physik*, 2, 178, 1920
- Demus D, Goodby J, Gray GW, Spiess, HW. and Vill, V,(1998), "Handbook of Liquid Crystals", vol. 1, *Fundamentals*, Wiley-VCH, Germany, p. 217.
- Dimitriev VG., Gurzadyan GG and Nikogosyan, DN (2010), *Handbook of Nonlinear Optical Crystals*, Berlin and Heidelberg, Springer-Verlag
- Dominguez A, Fernandez A, Gonzalez N, Iglesias E, Montenegro L (1997) "Determination of Critical Micelle Concentration of Some Surfactants by Three Techniques", *Journal of Chemical Education*, 74(10):1227-1231.
- Emmanuel I, Iwuoha, Malcolm R. Smyth, (2003), "Reactivities of organic phase biosensors: 6. Square-wave and differential pulse studies of genetically engineered cytochrome P450cam (CYP101) bioelectrodes in selected solvents" *Biosensors and Bioelectronics* 18, 237/244
- Ferrarini A, Gottarelli E, Nordio PL and Spada GP,(1999), Determination of absolute configuration of helicenes and related biaryls from calculation of helical twisting powers by the surface chirality model, *J. Chem. Soc. Perkin Trans. 2*, 3, 411-417.
- Filho AA, Laverd Jr A, Fujiwara F (2003) "Observation of Two Biaxial Nematic Mesophases in the Tetradecyltrimethylammonium Bromide/Decanol/Water System", *Langmuir*, 19:1127-1132.
- Freiser MJ (1970) "Ordered States of a Nematic Liquid Crystals", *Physical review letters*, 24:1041-1043.

- Figueiredo Neto AM; Galerne Y, Liebert L, (1985). Cholesterization of a biaxial nematic lyomesophase studied by X-ray diffraction and optical microscopy. *J. Phys. Chem.* 1985, 89, 3939–3941.
- Galerne Y, Marcerou JP, (1983) “Temperature behavior of the order-parameter invariants in the uniaxial and biaxial nematic phases of a lyotropic liquid crystal.” *Phys Rev Lett.*; 51:2109–2111
- Garcia-Mateos I, Velazquez M, Rodriguez L (1990) “Critical micelle concentration determination in binary mixtures of ionic surfactants by deconvolution of conductivity/concentration curves”, *Langmuir*, 6(6):1078-1083.
- George H, Heilmeyer and Joel E, (1968), ”A new electric-field-controlled reflective optical storage effect in mixed-liquid crystal systems”, *Goldmacher Appl. Phys. Lett.* 13, 132
- Gottarelli G, Mariani P, Spada GP, Samori B, Forni A, Solladie G, and Hibert M, (1983), “Induction of cholesteric mesophases in nematic liquid crystals, and correlation of absolute configurations of some chiral oxiranes and thiiranes” *Tetrahedron*, 39, 1337-1344.
- Gottarelli G, Hibert M, Samori B, Solladie G, Spada GP and Zimmermann R, (1983), “Induction of the cholesteric mesophase in nematic liquid crystals: mechanism and application to the determination of bridged biaryl configurations”, *J. Am. Chem. Soc.*, 105, 7318-7321.
- Kunieda H, and Shinoda K, (1978), “Solution behavior of dialkyldimethylammonium chloride in water. Basic properties of antistatic fabric softeners”, *J. Phys. Chem.* 82: 1710
- Hamley IW , Pople JA, Fairclough JPA, Terrill NJ, Ryan AJ, Booth G, Yu E, Diat O, Almdal K, Mortensen K, and Vigild M. (1998). “Effect of shear on cubic phases in gels of a diblock copolymer” *J. Chem. Phys.* 108, 6929.
- Israelachvili, J, (1992), Third Edition, *Intermolecular and Surface Forces* J.N. Israelachvili
- Kleman M and Lavrentovich (2006) “Topological point defects in nematic liquid crystals”, *Philosophical Magazine*, 86, 4117-4137.
- Senyuk B, Kim YK, Tortora L, Shin ST, Shiyanovskii SV, Lavrentovich OD (2011) “Surface Alignment, Anchoring Transitions, Optical Properties and Topological Defects in Nematic Bent-Core Materials C7 and C12”, *Molecular Crystals Liquid Crystals*, 540, 20-41.
- Kooij FM and Lekkerkerker H (2000) “Liquid-Crystal Phases Formed in Mixed Suspensions of Rod- and Platelike Colloids”, *Langmuir*, 16:10144-10149.

- Kroin T, Figueiredo Neto AM, Liébert L, & Galerne, Y (1989). "Chirality-induced biaxiality at the uniaxial-to-biaxial cholesteric phase transition." *Physical Review A*, 40(8), 4647-4651.
- Kuball, HG, and Türk O, (1999), "Helical twisting power and circular dichroism as chirality observations - Development of a sector rule for the intermolecular chirality transfer in a liquid crystal phase." *Polish. J. Chem.*, 73, 209-228.
- Liébert L and Figueiredo Neto AM (1984), "Optical microscopic observation of depletion layers, in a calamitic ferronematic lyomesophase", *J. Phys. (Paris) Lett.* 45, L-173.
- Lawson KD, and Flautt, TJ, (1967), "Magnetically oriented lyotropic liquid crystalline phases." *J. Am. Chem. Soc.*, 89, 5489-5491.
- Lee H and Labes M (1984) "Helical Twisting Power of Amino Acids in a Nematic Lyophase", *Molecular Liquid Crystals*, 108(1-2):125-132.
- Lin SY, Lin YY, Chen, EM, Hsu CT, Kwan CC (1999) "A Study of the Equilibrium Surface Tension and the Critical Micelle Concentration of Mixed Surfactant Solutions", *Langmuir*, 15(13):4370-4376.
- London F, (1930), "Zur theorie und systematik der molekularkräfte" *Z. Physics*, 63, 245.
- Marcondes Helene ME, Figueiredo Neto AM, (1988) Topology of a surface of the phase diagram of the cholesteric lyotropic mesophase: potassium laurate/1-decanol/water/1-N-lauroyl potassium alaninate. *Mol. Cryst. Liq. Cryst. Incorporating Nonlinear Opt.* 1988, 162, 127– 138;
- Maier W, & Saupe A, (1958). Eine einfache molekulare Theorie des nematischen kristallinflüssigen Zustandes. *Zeitschrift Für Naturforschung A*, 13(7).
- Lehmann M, (2009) "The Dawn In The Area Of Thermotropic Biaxial Nematics." *Liquid Crystals Today*, 18(1), 31-34,
- Simoes M, Et. Al.,(2019) "Optical Signal and Optical Axes in Uniaxial and Biaxial Nematic Phases, Phase Transitions." 92(2), 117-125,
- PGd e Gennes and Prost J, (1993). *The Physics of Liquid Crystals*, Second Edition, Oxford University Press, Oxford.
- Photinos P, Melnik G, and Saupe A, (1986) "Electric conductivity measurements on the nematic states of a micellar solution of potassium laurate/1-decanol/D2O" *J. Chem. Phys.* 84, 6928
- Palffy-Muhoray P, De Bruyn J, Dunmur D (1985) "Phase behavior of binary nematic liquid crystal mixtures", *The Journal of chemical physics*, 82:5294-5295.

- Pape M. and Hiltrop K, (1997), "Influence of lyotropic nematic host phases on the twisting power of chiral dopants." *Mol. Cryst. Liq. Cryst.*, 307, 155-173.
- Partyka, J. and Hiltrop K, (1996), "Chirality induction in lyotropic nematic liquid crystals." *Liq. Cryst.* 20, 611-618.
- Radley K, & Saupe A (1978). "Cholesteric states of micellar solutions." *Molecular Physics*, 35(5), 1405-1412.
- Radley K and Cattey H (1992) "Amphiphilic cholesteric liquid crystals prepared from the quaternary ammonium surfactant S-(–)-1-hexadecyl-1-methyl-2-pyrrolidinemethanol bromide", *Liquid Crystals*, 12(5):875-878.
- Ranjesh, A, Alipanah, Z, Kiani, S, Zakerhamidi, MS, & Yoon, TH (2019). "A method to find the initial temperature range of the short-range order in the isotropic phase of nematic liquid crystals based on the electro-optical Kerr effect." *Journal of Molecular Liquids*, 274, 646-652.
- Reinitzer, Friedrich. Contributions to the knowledge of cholesterol AU-Liquid Crystals, 5(1), 7-18.
- Reis D, Akpınar E, Neto AMF (2013) "Effect of Alkyl Chain Length of Alcohols on Cholesteric Uniaxial to Cholesteric Biaxial Phase Transitions in a Potassium Laurate/Alcohol/Potassium Sulfate/Water/Brucine Lyotropic Mixture: Evidence of a First-Order Phase Transition", *The Journal of Physical Chemistry B*, 117:942-948.
- Rosevear FB, 1968, Liquid crystals- "Mesomorphic phases of surfactant compositions". *J. Soc. Cosmet. Chem.*, 19, 581-594.
- S Chandrasekhar (1977). *Liquid Crystals*, Second Edition, Cambridge University Press, Cambridge.
- Santoro PA, Sampaio AR, da Luz HLF, "Temperature dependence of refractive indices near uniaxial biaxialnematic phase transition." *Phys Lett A*. 2006; 353:512–515
- Salem JK, El-Nahhal I, Najri B, Hammad T, Kodeh F (2016) "Effect of anionic surfactants on the surface plasmon resonance band of silver nanoparticles: Determination of critical micelle concentration", *Journal of Molecular Liquids*, 223:771-774.
- Serra F (2016) "Curvature and defects in nematic liquid crystals", *Liquid Crystals*, 43, 1920-1936.
- Singh SAD, Professor David A. (2002), First Edition, *Liquid Crystals*.
- Stroobants A and Lekkerkerker H (1984) "Liquid crystal phase transitions in a solution of rodlike and disklike particles", *The Journal of Physical Chemistry*, 88:3669-3674.

- Stoiber RE, and Morse SA, "Crystal Identification with the Polarizing Microscope." Chapman & Hall, New York, 1994
- Sutherland RL, (1996), Handbook of Nonlinear Optics, Marcel Dekker, New York.
- Tracey AS and Radley K, 1984,"Effects of composition on cholesteric behavior in the lyotropic mesophase system of potassium N-dodecanoyl-L-alaninate." J. Phys. Chem., 88, 6044-6048.
- Wahlstrom EE, Optical Crystallography, John Wiley & Sons, Inc., New York, 4th edn, 1969
- White DL, and Feldman M, (1970), "Liquid-crystal light valves." Electron. Lett. 6, 837
- Quist PO (1995) "First order transitions to a lyotropic biaxial nematic", Liquid Crystals, 18:623-629.
- Y Hendriks, J Charvolin, and M Rawiso (1986), "Uniaxial-biaxial phase transition in lyotropic nematic solutions: Local biaxiality in the uniaxial phase" Phys. Rev. B 33, 3534
- Y Galerne, A M Figueiredo Neto, and L Li´ebert (1987), "Microscopical structure of the uniaxial and biaxial lyotropic nematics" J. Chem. Phys. 87, 1851.
- Yeh P and Gu C (1999), Optics of liquid crystal displays, Second Edition, Wiley, New York
- Yiming Huang and Shuangying Gui,(2018), "Factors affecting the structure of lyotropic liquid crystals and the correlation between structure and drug diffusion", RSC Adv., 2018, 8, 6978 DOI: 10.1039/c7ra12008g
- Yu. K. Kornienko and Fedchuk AP, (1997), "Role of different polarization mechanisms in the self-organization of the director of a thin layer of nematic liquid crystal", Zh. Tekh. Fiz. 67, 23–28
- Yu LJ, & Saupé A, (1980)."Observation of a Biaxial Nematic Phase in Potassium Laurate-1-Decanol-Water Mixtures." Physical Review Letters, 45(12), 1000-1003.
- Zajac J, Chorro C, Lindheimer M, Partyka S,"Thermodynamics of micellization and adsorption of zwitterionic surfactants in aqueous media." Langmuir 1997, 13, 1486–1495.
- Zharkovaa GM, Kovrizhinaa VN, and Petrov AP, (2018), " Panoramic temperature, pressure, and shear stress sensors based on liquid crystal composites" issn 1811-2382, polymer science, series c, 2018, vol. 60, no. 1, pp. 14–22.

Zana R, Marinov G, and, Michels B, (1998), “Dynamics of Micelles of Poly (ethylene oxide) –Poly (propylene oxide) –Poly (ethylene oxide) Block Copolymers in Aqueous Solutions”, *Langmuir*, 14, 2639

Zhou T, & Zhao J, (2009). “Synthesis and thermotropic liquid crystalline properties of zwitterionic gemini surfactants containing a quaternary ammonium and a sulfate group.” *Journal of Colloid and Interface Science*, 338(1), 156-162.

J Israelachvili, *Intermolecular and Surface Forces*, First Edition Academic Press, London, 1985



7. CURRICULUM VITAE

Name SURNAME : Seda Uyanık

Place and Date of Birth : 27/04/1992

Universities

Bachelor's Degree : Abant Izzet Baysal University

e-mail : seda.uyanik@hotmail.com

Address : Bolu Abant Izzet Baysal University, Science
& Art Faculty, Gököy Campus, BOLU

List of Publications :

Congresses :

26 – 27 April 2018 International Eurasian Conference on Biological and
Chemical Sciences

4 - 6 October 2018 International symposium on Graduate Research in
Science

16 - 18 May 2017 National Chemistry Students Congress